Systems/Circuits

Complex Effects on *In Vivo* Visual Responses by Specific Projections from Mouse Cortical Layer 6 to Dorsal Lateral Geniculate Nucleus

Daniel J. Denman and Diego Contreras
Department of Neuroscience, University of Pennsylvania Perelman School of Medicine, Philadelphia, Pennsylvania 19104

Understanding the role of corticothalamic projections in shaping visual response properties in the thalamus has been a longstanding challenge in visual neuroscience. Here, we take advantage of the cell-type specificity of a transgenic mouse line, the GN220-Ntsr1 Cre line, to manipulate selectively the activity of a layer 6 (L6) corticogeniculate population while recording visual responses in the dorsal lateral geniculate nucleus (dLGN). Although driving Ntsr1 projection input resulted in reliable reduction in evoked spike count of dLGN neurons, removing these same projections resulted in both increases and decreases in visually evoked spike count. Both increases and decreases are contrast dependent and the sign is consistent over the full range of contrasts. Tuning properties suggest wide convergence of Ntsr1 cells with similar spatial and temporal frequency tuning onto single dLGN cells and we did not find evidence that Ntsr1 cells sharpen spatiotemporal filtering. These nonspecific changes occur independently of changes in burst frequency, indicating that Ntsr1 corticogeniculate activity can result in both net excitation and net inhibition.

Key words: **corticothalamic; gain; *in vivo*; layer 6; Ntsr1; thalamus**

Introduction

In most sensory modalities, the primary sensory thalamus is the locus of information transfer from the sensory periphery to cortex (Jones, 2007). Reciprocal projections from primary sensory cortex to thalamus are in a position to shape this transfer: corticothalamic (CT) axons make excitatory synaptic connections with thalamocortical relay cells at distal metabotropic glutamate synapses (McCormick and von Krosigk, 1992), as well as with the thalamic inhibitory neurons of the reticular nucleus (RE) and any present thalamic inhibitory interneurons (Bourassa and Deschênes, 1995; Zhang and Deschênes, 1997, Steriade and Deschênes, 1984; Jones, 2007, Jurgens et al., 2012). Indeed, whereas electrical stimulation of the cortex results in a predominantly inhibitory response in TC cells *in vivo* (Contreras and Steriade, 1996; Destexhe et al., 1998) and *in vitro* (Crunelli et al., 1988), functional studies have concluded that the primary visual cortical influence (V1) on dorsal lateral geniculate nucleus (dLGN) is facilitatory (Przybyszewski et al., 2000), suppressive (Andolina et al., 2007), or both (Kalil and Chase, 1970; Molotchnikoff and Lachapelle, 1977; McClurkin et al., 1994), whereas still others see minimal effects on responses (Richard et al., 1975; Baker and Malpeli, 1977).

Reciprocal CT projections originate in cortical layer 6 (L6) from pyramidal neurons that have an apical dendrite extending to L4 and a bifurcating axon that terminates in both L4 and the thalamus (Tombol, 1984; Zhang and Deschênes, 1997; Zarrinpar and Callaway, 2006; Briggs, 2010; Thomson, 2010). In L6 of V1, CT cells are intermixed with claustrum-projecting, pulvinar-projecting, cortical-projecting, and local cortical neurons (Zarrinpar and Callaway, 2006; for review, see Briggs, 2010; Thomson, 2010). Most techniques for manipulating CT activity have included mixed L6 populations (Hull, 1968; Baker and Malpeli, 1977; Sillito et al., 1994; de Labra et al., 2007). Investigations of the effect of V1 CT axons on dLGN activity have yielded potential roles for this projection in gain control (Przybyszewski et al., 2000), responsiveness to high-velocity stimuli (Gulyás et al., 1990), sharpening of receptive fields (RFs) (Marrocco and McClurkin, 1985; Andolina et al., 2013), and increasing reliability and precision of spike timing (Wörgötter et al., 1998; Andolina et al., 2007).

Transgenic approaches allow for manipulation of genetically specified populations of neurons and have facilitated investigation of the role of L6 CT neurons (Olsen et al., 2012). Rapid, bidirectional modification of CT cell activity via optogenetics could yield new insight into the function of CT input and the cell types responsible for previously observed CT effects. Here, we use the GN220 Ntsr1-Cre l mouse line (Gong et al., 2007, Olsen et al., 2012) to investigate the effect of CT cells on dLGN responses. We find that removing Ntsr1 activity was capable of driving both increases and decreases in visually evoked spike count, even in simultaneously recorded cells, without affecting burst frequency. The effect is contrast dependent; tuning properties suggest wide

Received Jan. 5, 2015; revised April 7, 2015; accepted April 11, 2015.

Author contributions: D.J.D. and D.C. designed research; D.J.D. performed research; D.J.D. analyzed data; D.J.D. and D.C. wrote the paper.

This work was supported by the National Eye Institute–National Institutes of Health (Grant R01 EY020765) and the University of Pennsylvania (Vision Training Grant 2T32EY00735). We thank Larry Palmer for help in stimulus generation and data interpretation.

The authors declare no competing financial interests.

Correspondence should be addressed to Diego Contreras, Department of Neuroscience, University of Pennsylvania School of Medicine, 215 Stemmler Hall, Philadelphia, PA 19106-6074. E-mail: diegoc@mail.med.upenn.edu.

DOI:10.1523/JNEUROSCI.0027-15.2015

 0270-6474/15/359265-16$15.00/0

convergence of Ntsr1 cells with similar spatial and temporal frequency tuning onto single dLGN cells. We did not find evidence that Ntsr1 cells sharpen spatial tuning properties or improve temporal fidelity.

Materials and Methods

Procedures. All procedures were approved by the University of Pennsylvania Institutional Animal Care and Use Committee using adult GN220 Ntsr1-Cre mice originally generated by the GENSAT project (Gong et al., 2007).

Expression of opsins. To achieve specific expression of microbial opsins in Ntsr1 cells, we used an adeno-associated viral (AAV) delivery system and the FLEX switch (Atasoy et al., 2008) to limit expression to Cre^+ cells (Cardin et al., 2010b). Briefly, animals of either sex were anesthetized with 2% inhaled isoflurane and placed in the stereotactic apparatus. A burrhole craniotomy was made over V1. A Hamilton syringe with a 33 gauge beveled opening needle controlled by a Quintessential Stereotactic Injector (Stoelting) was inserted into V1 to a tip depth of 900 μm. After a 10 min rest period, 300–1000 nl of AAV (serotype: 2/9, prepared by the University of Pennsylvania Vector Core) was injected at a rate of 30 nl/min. After another 10 min rest period, the syringe was retracted, the burrhole filled with bone wax, and the skin sutured. At least 2 weeks elapsed before acute recording to allow for maximal opsin expression.

Acute experiment preparation. All data were collected during acute recording sessions. Animals were anesthetized with 2% inhaled isoflurane and placed in the stereotactic apparatus. Temperature was maintained at 37°C via feedback to a heating pad from a rectal thermometer and eye moisture maintained via transparent lubricant. A cranial window was opened over dLGN and V1. An array of independently positionable tetrodes (Thomas Recording) was lowered into cortex above dLGN and a laser-coupled optical fiber positioned on the cortical surface above V1. Each tetrode was lowered individually; placement in dLGN was assessed by strong multiunit spike modulation to a spatially uniform flashed stimulus. Because L6 cortical activity can be sensitive to many anesthetic regimes (Angel and LeBeau, 1992; Briggs and Usrey, 2008), once tetrodes were positioned, the isoflurane concentration was lowered (~1.2%) and continuously adjusted based on the synchrony of the local field potential activity. This ensured a cortical state with relatively little slow oscillation and an activated pattern (Steriade, 2001) to facilitate L6 responsiveness. In a previous study, careful monitoring of anesthetic state to maintain an EEG-activated pattern resulted in visual responses that were virtually undistinguishable from those of awake animals (Denman and Contreras, 2014).

Stimulation and acquisition. Spike data were acquired at 30.303 kHz, filtered between 600 and 6000 Hz, and a threshold was manually set on each channel. Crossing of this threshold triggered acquisition of the spike waveform on all four tetrode channels.

Visual stimuli were generated using the ViSaGe stimulus generation hardware (Cambridge Research Systems) and a custom software package using the Cambridge Research Systems-provided MATLAB toolbox. Stimuli were presented on a 19-inch cathode ray tube monitor configured to refresh at 100 Hz with 600 × 800 resolution. The monitor was placed 30 cm from the eye and the position in the animal's visual field was adjusted in an attempt to maximize the evoked activity from a single recording site. Drifting grating stimuli subtended a total of ~70° of visual space and were presented with at least 1 s of mean luminance between each stimulus. Ternary noise stimuli contained 12 × 16 square pixels with an edge length of 3.3 degrees. Each frame was independent of the previous and frames changed at a rate of 50 Hz. The spatially uniform flicker stimulus was designed according to previously published methods (Reinagel and Reid, 2000; Kumbhani et al., 2007), modified here to draw the contrast value randomly from an even distribution. The stimulus was updated at 50 Hz and a 5 s sample was repeated 100 times for each condition.

Laser illumination was performed using either a 200W, 532 nm solid state laser (for Arch activation) or 100W, 473 nM laser (for ChR2 activation) (OptoEngine) coupled to a bare 200 μm, 0.62 numerical aperture (NA) optical fiber. We chose a higher NA aperture fiber to maximize the horizontal spread of our laser illumination to achieve maximal coverage of V1 during the optogenetic manipulation. Laser illumination followed one of two protocols: either synchronous (see Figs. 1, 3), in which the laser was activated on the first frame of a visual stimulus and maintained throughout, or enveloping (see Figs. 2, 4, 5, 6, 7, 8, 9, and 10), in which the laser was activated 200–500 ms before the onset of stimulation and remained activated until the same amount of time after presentation of the stimulus. In both cases, laser power was maintained constant for the duration of illumination.

Analysis. Spike waveforms were clustered offline using a mixture of an initial algorithmic (KlustaKwik) sorting followed by manual refinement using SpikeSort 3D (Neuralynx), as described previously (Denman and Contreras, 2014).

Spike counts were made over the period during which the stimulus (drifting grating, ternary noise, or flicker) was present on the display plus 200 ms to include any offset transients. The Ntsr1 effect was measured as the normalized difference between control and laser (Arch or ChR2) activated conditions as follows:

$$Nstr1\ effect = \frac{N_{\text{laser}} - N_{\text{control}}}{N_{\text{control}}}$$

where N_{laser} is the spike count during Ntsr1 cell manipulation and N_{control} is the spike count during control conditions.

Contrast response functions (CRFs) were measured using the F1 component as the measure of each dLGN unit's spiking response or as normalized Ntsr1 effect (see above) as a function of contrast. CRFs were fit with a hyperbolic ratio function, as in Contreras and Palmer, 2003 as follows:

$$f(C) = R_0 + R_{\max} * \left(\frac{C^n}{(C_{50}^n + C^n)}\right)$$

where R_0 is an offset, $R_{\max}$ is the amplitude, C_{50} is the inflection point, and n controls the slope of the fit.

The orientation tuning curves, across the range 0–360°, were fit with the von Mises function (Swindale, 1998) as follows:

$$f(\theta) = b_0 + b_1 e^{K(\cos(\theta-\mu)-1)} + b_2 e^{K(\cos(\theta-\mu+\pi)-1)}$$

where b_0 is an offset for the baseline firing rate, b_1 and b_2 independently determine the size of each peak, K is the width parameter, and μ the preferred orientation. The orientation selectivity index (OSI) was calculated from raw responses as the difference between responses at preferred and orthogonal orientations as follows:

$$OSI = \frac{R_{\text{preferred}} - R_{\text{ortho}}}{R_{\text{preferred}} + R_{\text{ortho}}}$$

where $R_{\text{preferred}}$ is the response at the preferred orientation, as determined by the circular Gaussian fit, and R_{ortho} is the response at the orientation 90° from $R_{\text{preferred}}$.

Spatial and temporal frequency tuning curves were generated from spike counts and both fit with the same function, from Gao et al., 2010 as follows:

$$f(x) = B + Ae^{\frac{-1}{2s^2} * log\left(\frac{x+0}{p+0}\right)^2}$$

where B is an offset for the baseline firing rate, A is the amplitude, s is the SD, O is the log offset, and p the preferred spatial or temporal frequency.

Spatial RFs were fit with a 2D Gaussian function as follows:

$$f(x, y) = Ae^{\left[\frac{-1}{2(1-cor)^2}\left(\left(\frac{x-x_0}{xWidth}\right)^2 + \left(\frac{y-y_0}{yWidth}\right)^2 - \frac{2*cor*(x-x_0)(y-y_0)}{xWidth*yWidth}\right)\right]}$$

with a center point chosen based on the pixel with maximal absolute deviation and the fit performed on the frame that included this pixel. Frames were computed at 10 ms intervals ($\Delta\tau$ = 10 ms). Although the RFs were mostly symmetrical, we allowed the x and y parameters to be independent to get the best possible fits.

Results

We investigated the role of corticogeniculate projections in modulating the visual responses of dLGN neurons using the GN220 Ntsr1-Cre transgenic mouse created by the GENSAT

project (Gong et al., 2007). To achieve fast, reversible inactivation of corticogeniculate neurons, we introduced GFP-Archaerhosopsin-3 (Arch; Chow et al., 2010) using a FLEX expression system (Atasoy et al., 2008; Chow et al., 2010) via intracranial injection of an AAV (Cardin et al., 2010b) ($n = 28$). In a subset of experiments ($n = 5$), we also introduced a FLEXed mCherry-Channelrhodopsin-2 (ChR2) virally into the opposite hemisphere of Ntsr1-Cre mice to activate Ntsr1 cells specifically (see Materials and Methods). Expression of opsins was limited to a CT neuron population (Figs. 1*A*, 2*A*), which we will refer from here on as Ntsr1 cells. Expression of opsins after viral injections was extensive, covering all of V1; somatic expression was restricted to the lower layers of V1 and robust expression can be seen in axonal terminals in LGN and RE (Figs. 1*A*, 2*A*). Ntsr1 cells were limited to L6 (Figs. 1*A*, 2*A*), neurites expressing the fluorescent reporter extended to L4 and were densely ramified, and a subset also extended to and were ramified in L1 (Figs. 1*A*, 2*A*). We also observed axonal projections from Nstr1 cells to the lateral dorsal nucleus and lateral posterior nucleus of the thalamus. In target structures, as well as cortical L4, the density of neurites was such that gaps in fluorescence that shape somas were observable. To record visually evoked spiking activity from small populations of neurons in dLGN and V1, we used arrays of independently movable tetrodes. Individual units were clustered manually from tetrode recordings by defining boundaries in waveform feature spaces (example recording: Fig. 1*B*, left); up to seven units were identified on single tetrodes (example recording: Fig. 1*B*, right). To control the opsins in Nstr1 cells, we coupled a green (532 nm) or blue (473 nm) laser into an optical fiber positioned on the cortical surface; output wattage from the fiber tip was measured to be $\sim$50 mW/mm^2. We then investigated the effect of activating (with ChR2) or inactivating (with Arch) Ntsr1 cells on dLGN cell visual responses.

Driving Ntsr1 corticogeniculate cell activity reduces evoked dLGN spike count

V1 has been shown to enhance (Tsumoto et al., 1978; McClurkin et al., 1994, Przybyszewski et al., 2000), suppress (Tsumoto et al., 1978; McClurkin et al., 1994; Andolina et al., 2007, 2013), or have little effect on dLGN visually evoked activity (Richard et al., 1975; Baker and Malpeli, 1977). To assess directly the impact of Ntsr1 projections to dLGN, we injected a virus carrying ChR2 into GN220-Ntsr1 mice and recorded dLGN responses during direct Ntsr1$^+$ cell ChR2 excitation. Our injections yielded good coverage of the L6 Ntsr1 population (Fig. 1*A*). We then recorded thalamic activity during visual stimulation (optimized to drive mouse dLGN units: 0.08 cycles/degree, 3 degrees/s) either alone or paired with synchronous activation of the transfected Ntsr1 population with a blue laser (Fig. 1*C–F*, blue lines indicate ChR2 activation). Single dLGN units responded in both conditions with a temporally modulated firing output at the frequency of the grating. We quantified visual responses by the mean firing rate (the DC component) and the amplitude of the fundamental harmonic (the F1 component). This activation of Ntsr1 cells led to robust and reliable decreases in visually evoked spike count (Fig. 1*C*,*D*, two example cells, PSTH during ChR2 in blue) regardless of the strength of visual stimulation defined by the contrast of the sinusoidal grating (Fig. 1*E*,*F*, for the same two example cells, ChR2 in blue). Anecdotally, synchronous ChR2 activation of Nstr1 cells sometimes caused an initial burst or increase in spike count in dLGN units in the absence of a visual stimulus (Fig. 1*C*, left, asterisk), followed by reduced spike count during visual stimulation. We measured the effect of activation of ChR2 as the fold change in visual response (Fig. 1*G*,*H*). Overall ($n = 32$ neurons), spike count was significantly reduced in 23 cells by an average of 63%, whereas only one cell showed a significant increase in spike count and eight cells showed no significant changes in visual response firing rate (Fig. 1*G*,*H*). In sum, we find that synchronous activation of Ntsr1 input unambiguously elicits strong and sustained reduction in dLGN unit spike count in the majority of cells, presumably through activation of reticular or local inhibitory input to dLGN relay cells.

Removing Ntsr1 corticogeniculate cell activity has mixed effects on evoked dLGN spike count

To investigate dLGN responses in the absence of Ntsr1 cells, we expressed Arch widely across V1 and in LGN and RE terminals (Fig. 2*A*). In recordings of small groups of cells in L6, spontaneous activity of a subset of units (28%) was reduced by 532 nm light illuminating V1, whereas other nearby units were not affected directly (Fig. 2*B*). Activation of Arch in Ntsr1 cells effectively eliminated visually evoked activity in these cells, even at preferred orientations (Fig. 2*C*, gray: control, green: illumination with green laser). Overall, Arch activation eliminated the evoked response in 45% of the units recorded within L6 based on depth from cortical surface (Fig. 2*D*). We first investigated the effect of Nstr1 cell projections on dLGN spike counts evoked with drifting sinusoidal gratings.

Surprisingly, given the suppressive effect of activating Ntsr1 input, removing Ntsr1 input resulted in a range of effects on single dLGN unit visual responses (Fig. 3), exemplified by the representative units in Figure 3, *A–C*. On half of the presentations of an optimized grating, randomly interleaved, corticogeniculate Ntsr1 cells were hyperpolarized by illuminating the cortex with a green laser (532 nm), activating Arch and reducing Ntsr1 output (+Arch). The single dLGN unit in Figure 3*A* (average tetrode waveforms shown on top row) showed robust output to the drifting grating (represented above by dot rasters) both during control conditions (black) and +Arch conditions (green). This cell exemplifies the group of dLGN units that showed no changes in visual response in the absence of Ntsr1 input (DC: 14.3 $\pm$ 2.2 Hz in control, 12.4 $\pm$ 2.0 Hz +Arch; F1: 13.6 Hz in control, 12.3 Hz +Arch). In contrast, the unit in Figure 3*B* is an example of cell that showed an increase in response in the absence of Ntsr1 corticogeniculate input, in this case, a 42% increase in response (DC: 4.5 Hz in control; 6.4 Hz +Arch). Finally, the single dLGN unit in Figure 3*C* showed a 15% decrease in visual response in the absence of Ntsr1 input (DC: 4.9 Hz in control; 3.7 Hz +Arch; F1: 4.1 Hz in control; 3.5 Hz +Arch). To capture the diversity of effect in our population of cells, we plotted the DC (Fig. 3*D*) and F1 response components (Fig. 3*E*) of the response of all dLGN units before (control) and during activation of Arch in Ntsr1 cells (+Arch). The main effect of removing Ntsr1 input in spike output was a modest change in response magnitude with a nonsignificant tendency for an increase in the visual response (DC) compared with control responses.

To summarize the effects of removing Ntsr1 input on dLGN visual responses, we calculated the ratio between the response DC in control conditions and +Arch for each unit. The distribution of response ratios (Fig. 3*F*) had a mean of 1.24 $\pm$ 0.05 and a median of 1.09. The distribution shows that the visual response of 38% ($n = 46/122$) of dLGN units had no contribution from Ntsr1 corticogeniculate cells, because removing their input had no effect ($0.9 <$ response ratio < 1.1, Fig. 3*F*, vertical dotted lines). In contrast, in 21% ($n = 26/122$) of dLGN units, Ntsr1 input increased visual responses, because removing it decreased response

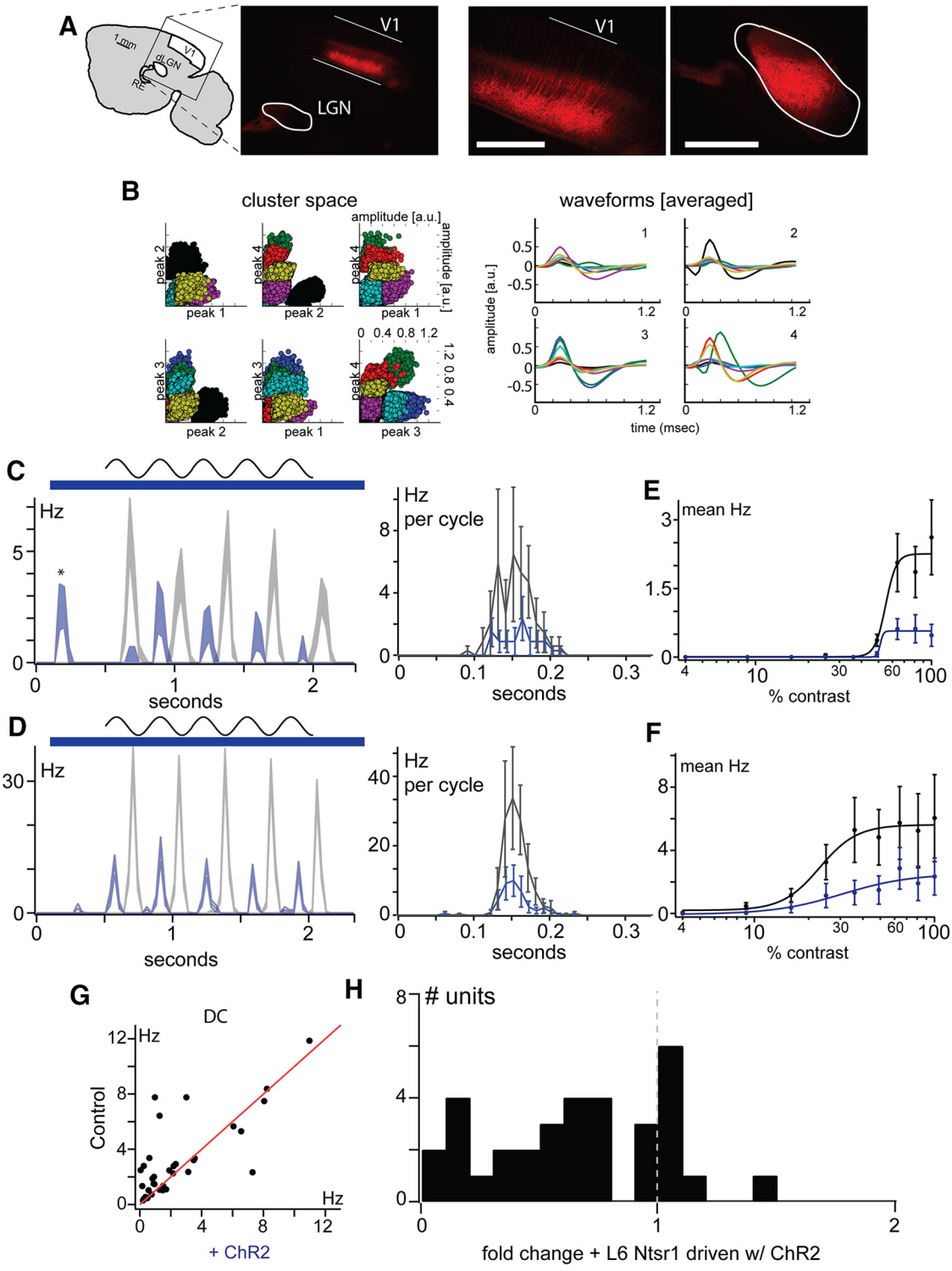

Figure 1. Effect of stimulating Ntsr1 cells on dLGN visual responses. ***A***, Expression of ChR2-mCherry in Ntsr1 neurons in L6 (left). Terminals are visible in cortical L4 (middle), RE, and dLGN (right). ***B***, Example clustering from a single tetrode LGN recording. Six feature spaces used to define clusters from this recording shown at left; individual spikes are color coded by cluster identity. The average waveform from each of these clusters is shown at right, color coded by the same identity as individual spikes in cluster spaces at left. ***C***, ***D***, Two example cells responding to a drifting grating (top) show a reduced response (blue traces) when the cortex is illuminated with blue light (blue bar) compared with control (gray traces). In the peristimulus time histograms at left in ***C***, the phase of the control stimulus and during blue light are different and therefore the responses are not superimposed; phase-aligned responses (right plots, cyclegrams) show consisted reduction across the response cycle. Both the number of spikes per cycle (right plots, cyclegrams) and number of spikes across successive cycles (left plots) are decreased. Note the burst induced by Ntsr1 activation in the cell shown in ***B***, marked with an asterisk. ***E***, ***F***, This decrease is present at all contrasts. ***G***, Scatterplot of the effect of driving Ntsr1 cells on the DC component of repossess. ***H***, Distribution of the fold change in visual responsiveness corresponding to ***G***.

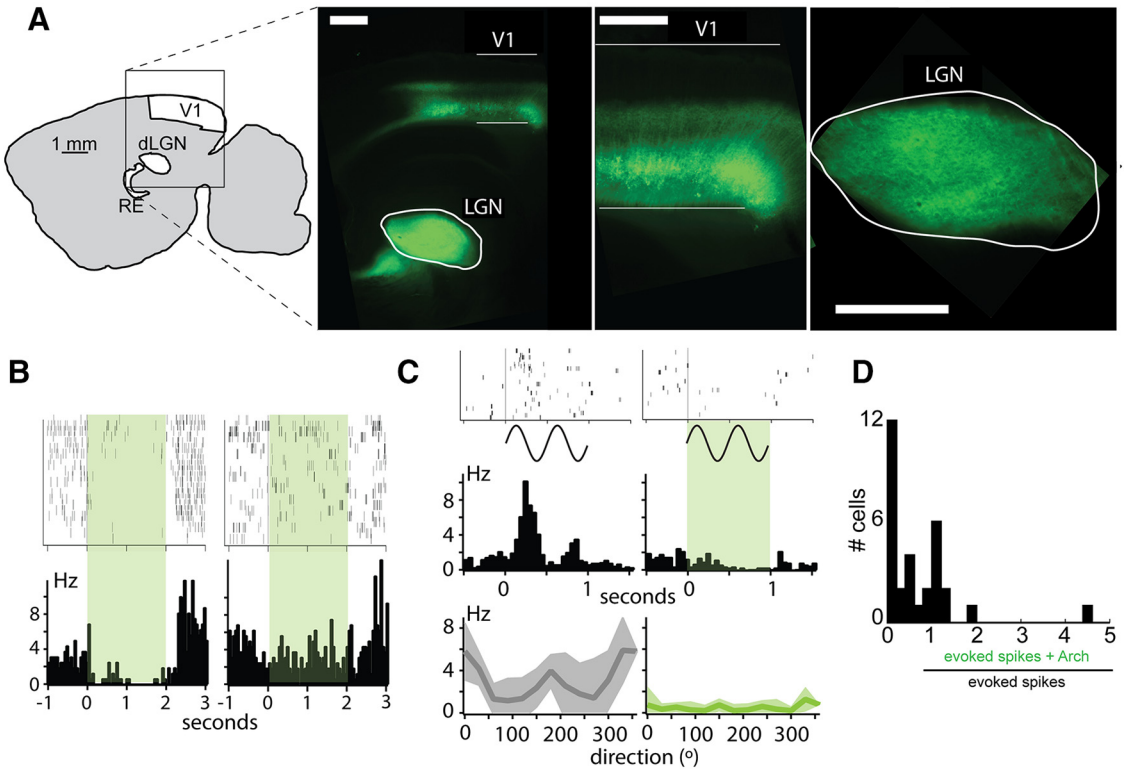

Figure 2. Optogenetic inactivation of L6 corticogeniculate cells. ***A***, Expression of Arch-GFP carried by an AAV 2/9 vector in Ntsr1-Cre mice injected directly into V1. Expression shown is 4 weeks after injection. Shown is a paraformaldehyde-fixed, sagittal section. Scale bar, 0.5 mm. ***B***, Reduction of spontaneous firing of cells in L6. Optical fiber is placed directly in V1; array of tetrodes lowered to approximate L6 depth (example shown: 712 μm). Spontaneous firing of a cell (left) is eliminated by activation of Arch; spontaneous activity of another cell recorded on the same tetrode (right) is unaffected by Arch. ***C***, Reduction of drifting grating evoked firing of a L6 cell. Two cycles of a drifting grating evoke a modulation response (left); enveloping activation of Arch eliminated the activity evoked by the same stimulus (right). ***D***, Distribution of the effect of activating Arch on visual stimulus evoked firing for single and multiclusters recorded in L6.

DC (minimum = 0.28). Finally, in 41% of dLGN units Ntsr1 input suppressed visual responses, because its removal led to increased response DC (maximum = 3.86). Noticeably, a small population had ratios centered around 2, which shows that, for some dLGN units, cortical input can reduce the visual response by ~50%.

The distribution of response ratio could be biased by very low or very high firing rates of dLGN units during control visual responses. Cells with high control firing rates could show small response ratios even for important effects of removing Ntsr1 input. Conversely, cells with low control firing rates could show very large response ratios even for small effects of Arch. To verify whether such bias was present in our data, we plotted the control firing rate (the numerator of the ratio) against the response ratio for all cells. The control firing rate (Fig. 3*G*, numerator) showed the same shape as the response ratio distribution, indicating that our distribution was not biased by the firing rates of the individual dLGN neurons. Such bias would have been apparent as a negative slope in the distribution of data points (larger rates = low ratios and vice-versa). For the vast majority of cells, the change in response DC (ΔDC) was larger than that of response F1 (ΔF1) (Fig. 3*H*).

Cortical input to the dLGN targets both interneurons and relay cells. In an attempt to determine whether the effect of removing Ntsr1 on each target is different, we separated our dLGN single unit population into two classes according to spike shape (Fig. 3*I*). Units with narrow spikes, such as the example in Figure 3*C*, were classified as fast-spiking (FS; 18/122) and are presumably interneurons (McCormick and Pape, 1990). The remainder of units (104/122) were classified as regular-spiking (RS), and are presumably relay neurons. Of our population of FS units, 33% showed reduced visual response in the absence of Ntsr1. Conversely, of all units that were suppressed (n = 29/137), 12% were classified as FS units (Fig. 3*I*). Units with the highest evoked firing rates behaved like the example cell in Figure 3*B*, showing modest suppression by Ntsr1 cells; evoked firing rate was otherwise not predictive of the type or magnitude of the effect (Fig. 3*J*). In sum, Ntsr1 cell projections can either modestly suppress or enhance both RS (relay) and FS (interneurons) dLGN unit responses.

Contrast dependence of Ntsr1 dLGN effects

It has been proposed that CT projections control the gain of dLGN responses (Przybyszewski et al., 2000) and that Ntsr1 cells mediate gain control in V1 (Olsen et al., 2012). Therefore, we hypothesized that dLGN sensitivity to increasing stimulus contrast should be affected by Ntsr1 activity. We first verified that the CRFs of our population of Ntsr1 cells were similar to those described previously in mouse V1 (Gao et al., 2010). We then measured the effect of removing Ntsr1 input on the CRFs of dLGN units using response F1. The effect of removing Ntsr1 input on the CRFs of dLGN units was again mixed (Fig. 4). As before (Fig. 3), we used the change in response magnitude to the highest contrast to separate our population into three groups: (1) cells with a larger than 10% increase (Fig. 4*A*, red, n = 24/109), (2) cells with a larger than 10% decrease (Fig. 4*A*, blue, n = 32/109), or (3) cells with a smaller than 10% change (Fig. 4*A*, black, 53/109) in the F1 response.

The example in Figure 4*B* is representative of those neurons in which removing Ntsr1 input increased the response to maximum contrast by >10%. The increase in response magnitude was contrast dependent; that is, it became larger at increasing stimulus contrast. The example cell in Figure 4*C* is representative of those

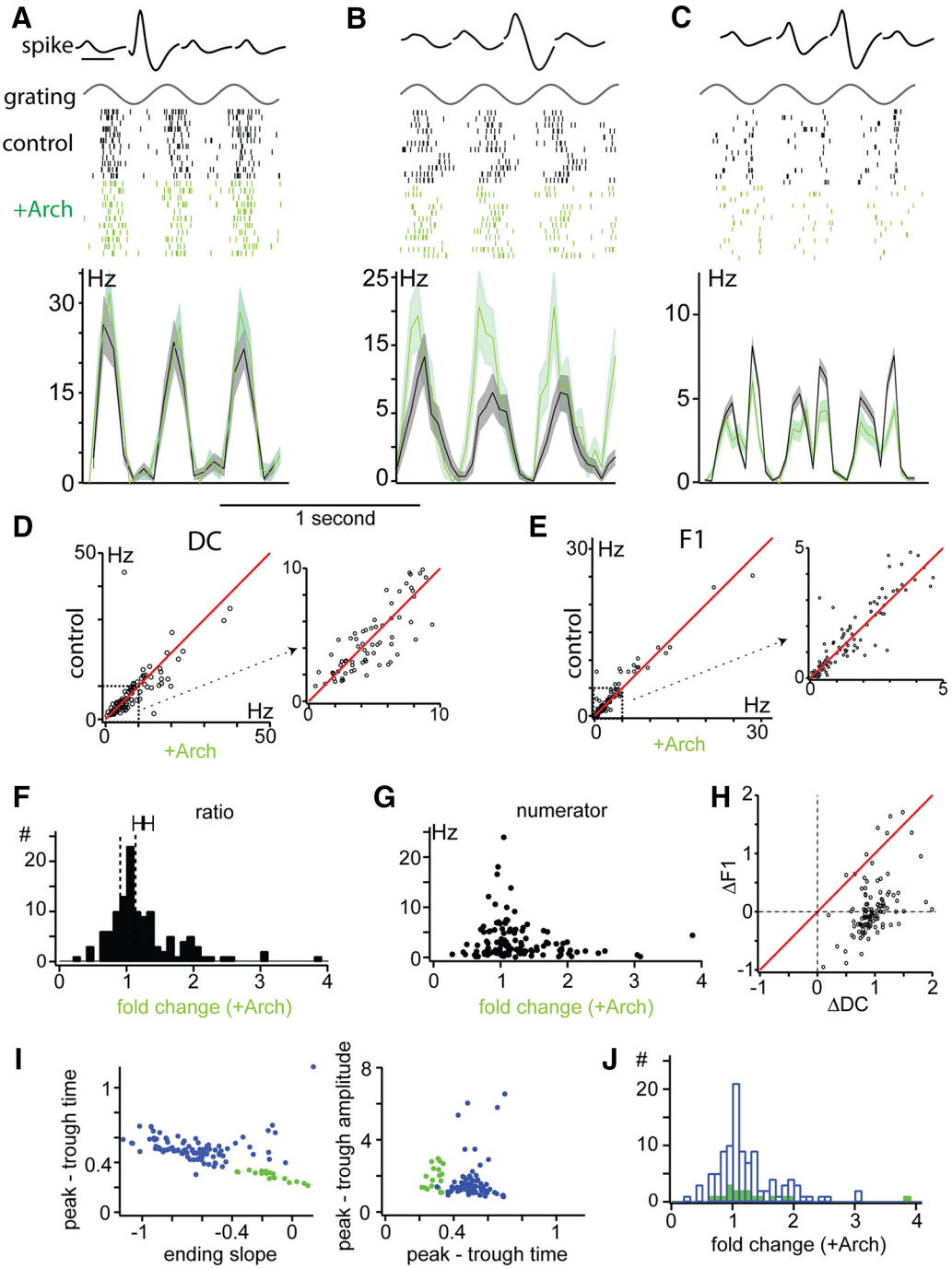

Figure 3. Effect of Ntsr1 cells on dLGN responses. ***A–C***, Examples of the effects of Ntsr1 cells on three dLGN single units. For each example, average waveforms for a single unit as seem on each of four tetrode wires is shown above the temporal envelope of the stimulus. Rasters for each of the three example single cells during control (black) and +Arch (green) trials are separated for clarity, but were presented interleaved. Peristimulus time histograms for each of the three example single units calculated with 33 ms bins for control (black) and +Arch (green) are shown with SEM for each bin shaded. ***D***, Scatter plot (left) of the effect of Ntsr1 cells on the DC component of dLGN responses to gratings. Right plot shows expansion of marked section in left plot. ***E***, Scatter plot (left) of the effect of Ntsr1 cells on the F1 component of dLGN responses to gratings. Right plot shows expansion of marked section in left plot. ***F***, Distribution of fold change in DC component without Ntsr1 cell activity. ***G***, Fold change in DC component is not dependent on high or low control firing rate. ***H***, Ntsr1 cell effect on the DC component (bottom) correlated with the magnitude of the effect on the F1 component (left). ***I***, Separation of dLGN single unit waveforms into RS (blue) and FS (green) according to peak-to-trough time, ending slope (left), and relative peak-to-trough amplitude (right). ***J***, Distribution of Ntsr1 cell effects is the same for putative RS and FS units.

neurons in which Ntsr1 had no effect along the entire range of stimulus contrast. Finally, the cell shown in Figure 4*D* showed the opposite effect: removing Ntsr1 input led to a decrease in visual response. Here again, the change in response magnitude was contrast dependent and occurred along the entire range of contrasts used. To compare across the population, we calculated the difference for each cell between the control CRF and +Arch. We averaged separately the difference CRF for all cells with an increase, an absence, or a decrease in response (Fig. 4*B–D*, right column) according to the 10% criteria described above. The comparison of the three averages (Fig. 4*E*) showed that both the increase and decrease in response magnitude was contrast dependent and spanned the contrast range used. Therefore, Ntsr1 input can control response gain in subpopulation of neurons, either upward or downward.

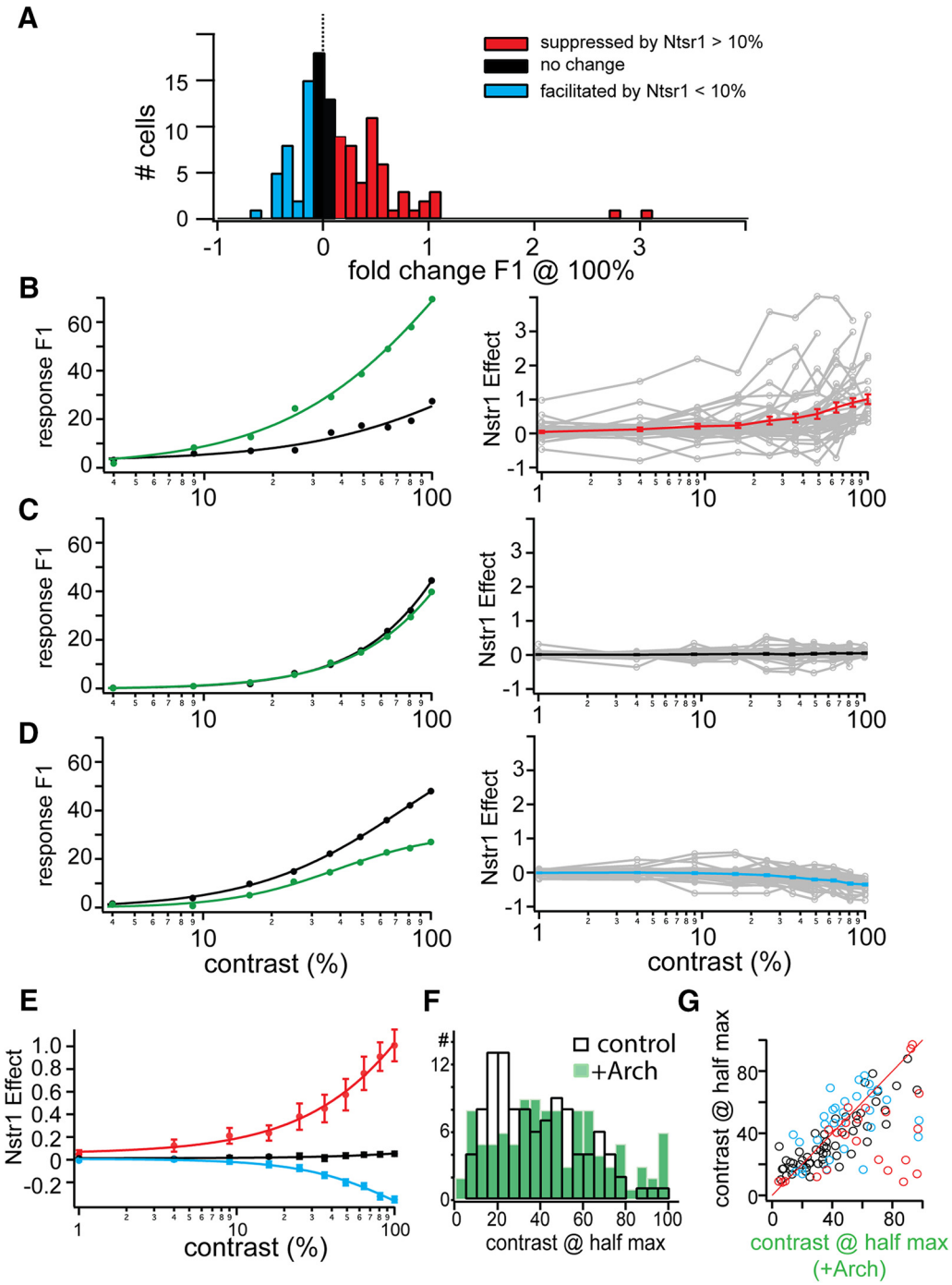

Figure 4. Contrast dependence of Ntsr1 cell effects on dLGN units. ***A***, Distribution of the fold change in the F1 component at 100% contrast. Individual units were sorted into suppressed by Ntsr1 (>10% increase in response, red), facilitated by Ntsr1 (> 10% decrease in response, blue), or unchanged by Ntsr1 (black). ***B–D***, Examples and sorted populations of units suppressed (***B***), unchanged (***C***), or facilitated (***D***) by Ntsr1 activity. For each group, an example unit with control (black) and + Arch (green) CRF is shown at left; all group CRFs, and the within-group average, is shown at right. ***E***, Within-group average CRFs from ***B–D*** plotted together. ***F***, Distribution of contrast at half-maximum response for control (open bars) and + Arch (green) conditions. ***G***, Scatter plot of data in ***F*** separated into suppressed (red), unchanged (black), and facilitated (red) by Ntsr1 groups.

To evaluate whether the dynamic range of the CRF changed in the absence of Ntsr1 input, we calculated the contrast at which the response F1 reached the 50% of its maximum. We found this to be more valuable for comparison across cells than the C50 from the hyperbolic ratio fits because many mouse dLGN CRFs do not saturate. Despite the changes in response magnitude, the value of contrast at 50% did not change after removal of Ntsr1 input. This was shown by the complete overlap of the two distributions (Fig. 4*F*, +Arch in green) and by plotting the values of individual cells in a scatter plot, which mostly aligned along the main diagonal (Fig. 4*G*).

In summary, we observed a stereotyped change in the CRF consistent with a gain change (Fig. 4*B–D*), such that Ntsr1 effects scale multiplicatively with contrast (Olsen et al., 2012). This multiplicative scaling could indicate that Ntsr1 cells implement gain control in dLGN; alternatively, Ntsr1 effects could follow global V1 gain changes (Carandini and Heeger, 2012; Carandini et al., 1997; Priebe and Ferster, 2012), possibilities that we cannot distinguish here.

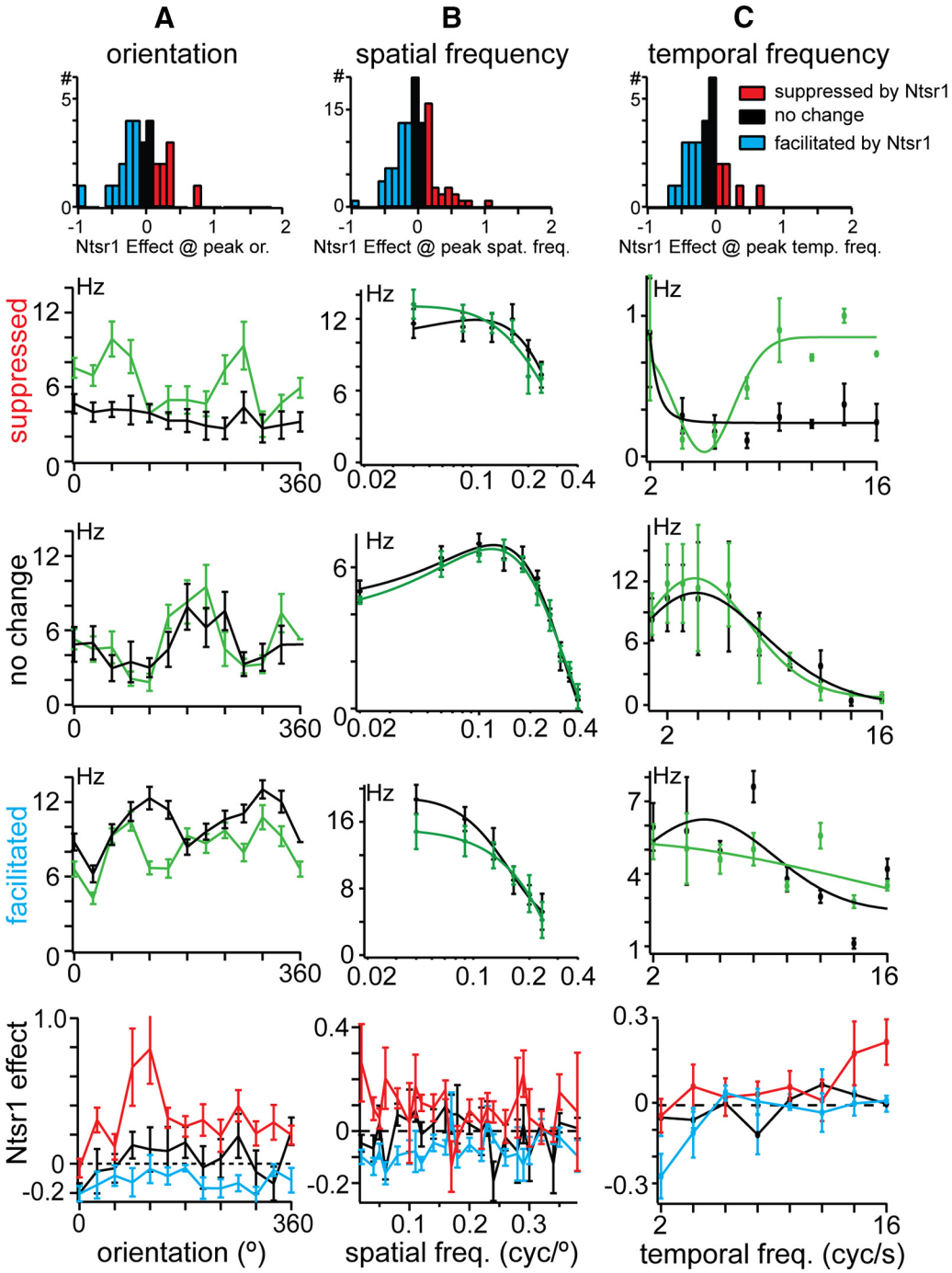

Figure 5. Effects of Ntsr1 cells across orientations, spatial frequencies, and temporal frequencies. ***A***, Distribution of the effects of Ntsr1 cells on response DC component (top); examples from each group of effect indicated in ***A***, suppressed (top), no change (middle), and facilitated (bottom); population averages for each group. ***B***, Same as ***A*** but for spatial frequency. ***C***, Same as ***A*** but for temporal frequency.

Convergence of Ntsr1 cell projections onto dLGN cells: effect on response selectivity

If similarly tuned Ntsr1 neurons project to a given dLGN cell, then the effects of removing Ntsr1 input on dLGN spike output should depend on the visual selectivity of Ntsr1 neurons. Therefore, we independently varied the orientation, spatial frequency, and temporal frequency of presented drifting gratings while interleaving trials with and without Ntsr1 input to dLGN (Fig. 5).

We measured orientation tuning in 28 dLGN units ($n = 4$ mice) and found that most cells in our population were untuned ($n = 18$, OSI < 0.33) or were weakly biased for orientation ($n = 9$, $0.33 <$ OSI < 0.66), consistent with other reports in mouse dLGN (Piscopo et al., 2013). Removing Ntsr1 input did not significantly alter OSI (mean OSI: 0.31 ± 0.02; +Arch mean OSI: 0.28 ± 0.02, $p = 0.18$, Wilcoxon signed-rank test) for either the untuned or the biased groups ($p > 0.05$, signed-rank test). We examined orientation-specific effects as we did with contrast, dividing cells into three groups based on the amplitude of the effect of removing Ntsr1 input at the stimulus orientation that causes the maximal response (Fig. 5*A*, top row). Of the 28 cells, eight showed no change (Fig. 5*A*, black), eight showed an increase (Fig. 5*A*, red), and 12 showed a decrease in response to best orientation

(Fig. 5*A*, blue). The example cell in Figure 5*B* showed a remarkable increase in response to the two orientations (OSI control = 0.08; OSI +Arch = 0.63) and exemplifies the one example for which orientation selective responses are suppressed by Ntsr1 input in control conditions. The two other groups are exemplified by a cell (Fig. 5*A*, third row) that showed a small orientation preference in control conditions and no change with Arch (OSI = 0.51, OSI +Arch = 0.53) and a cell in which its orientation bias was reduced in the absence of Ntsr1 input (Fig. 5*A*, fourth row; OSI = 0.42, OSI +Arch = 0.31). The average of all cells in each category (Fig. 5*A*, bottom row) showed no statistically significant effect of Ntsr1 input. This is consistent with the hypothesis that dLGN units receive input from Ntsr1 cells with a wide distribution of orientation preferences, suggesting wide convergence of Ntsr1 cells onto single dLGN cells.

We measured the effect of removing Ntsr1 input on the spatial frequency selectivity of dLGN neurons (Fig. 5*B*). We found that 28 cells showed an increase in peak spatial frequency (Fig. 5*B*, red), such as the example cell in Figure 5*B* (second row) in which the response to 0.02 cycles/degree increased by 1.9 spikes/s. Fifteen cells showed a decrease in peak spatial frequency (blue), such as the cell in Figure 5*B* (fourth row), which decreased by 3.9 spikes/s at the peak spatial frequency of 0.04 cycles/degree. Finally, 66 cells showed no change (black), such as the cell in Figure 5*B* (third row), which is a band-pass neuron with a peak spatial frequency of 0.1 cycles/degree. We found the spatial Ntsr1 effect to be the greatest at the lowest spatial frequencies, although some effect was observed across spatial frequencies.

Ntsr1 input also showed diverse effects on the temporal frequency tuning of dLGN neurons (Fig. 5*C*). As with orientation and spatial frequency, we classified our cells by the response to best stimulus in three groups: facilitated, no change, and suppressed (Fig. 5*C*, top row); 13/27 cells showed an increase in peak temporal frequency (red), 4/27 cells a decrease (blue), and 10/27 cells no change in peak temporal frequency +Arch (black). We illustrate these three groups by example cells in which the peak temporal frequency increased (Fig. 5*C*, second row, from 0.5 to 1.5 spikes/s at the peak temporal frequency of 14 cycles/s), decreased (Fig. 5*C*, fourth row; from 7.6 to 5.0 spikes/s at the peak temporal frequency of 8 cycles/s), or was not changed by removing Ntsr1 input (Fig. 4*C*, third row, peak temporal frequency was 4 cycles/s). The average of all cells in each group showed no significant effect at a particular temporal frequency. Notably, 4/25 cells showed strong release from inhibition at high (>10 Hz) temporal frequencies, which is consistent with a role for Ntsr1 cells suppressing dLGN activity at high temporal frequencies (Gulyás et al., 1990).

Using drifting gratings, we found that Ntsr1 cell suppression and facilitation occurs in the lower range of cortical spatial frequency tuning and is consistent across orientations and temporal frequencies. These results are consistent with a convergence of Ntsr1 inputs with diverse tuning properties onto single dLGN units.

Ntsr1 cells do not sharpen dLGN RF properties

Spatially extended drifting gratings could conceal spatially or temporally specific effects of corticogeniculate input. To investigate this possibility, we estimated spatiotemporal RFs of dLGN units using reverse correlation to dense ternary noise (Fig. 6). This stimulus provided the means to test the hypothesis that spatially distinct regions of Ntsr1 input provide opposite sign effects in dLGN. According to this hypothesis aligned areas enhance response and misaligned areas suppress dLGN responses (Tsumoto et al., 1978; Marrocco and McClurkin, 1985). In addition, this stimulus allowed us to test the hypothesis that Ntsr1 input ensures temporal organization among populations of visually responding dLGN neurons (Kalil and Chase, 1970; McClurkin et al., 1994; Sillito et al., 1994; Wörgötter et al., 1998).

RF size

Ternary noise yielded approximately circular ON- and OFF-center dLGN RFs with weak surrounds (Fig. 6*A*). To estimate the area of the RF center, we fit the reverse-correlated spatial RF at the time of the peak of the response with a 2D Gaussian (Fig. 6*B*; see Materials and Methods). Neither the RF area (Fig. 6*C*) nor the independent Gaussian width parameters (RF x and y, Fig. 6*D*) were significantly altered by Ntsr1 cell activity (x: $p = 0.30$; y: $p = 0.38$, Wilcoxon signed-rank tests).

RF response magnitude

The lack of change in RF size belies changes in the magnitude of both ON- and OFF-center responses in the absence of Ntsr1 input, as well as changes in the total number of spikes during noise presentation (Fig. 6*E*). The example cell in Figure 6*F* was a OFF-center cell for which removal of Ntsr1 input reduced both responses to center stimuli (i.e., the excitation produced by dark stimuli; Fig. 6*F*, left column, red represents a 10% increase in firing rate over background firing), as well as the inhibition produced by bright stimuli (Fig. 6*F*, right column, deep blue represents a 10% reduction in firing rate with respect to background). In this and all cells, the magnitude of the response was measured at the time of the peak (example cell peak = 100 ms). To quantify the effect of removing Ntsr1 input, we measured the change in response magnitude at each non-noise pixel of the RF center (Fig. 6*G*; see Materials and Methods). We found a significant reduction in the response to both increments and decrements in contrast. The excitatory response to dark was reduced by 41% [$p = 0.002$, Kolmogorov–Smirnov (K-S) test] and the inhibitory response to bright by 38% ($p = 0.001$; Fig. 6*G*, mean represented by dotted lines). Across the population (individual cells shown Fig. 6*H*, quantified below in *J*; $n = 32$), 26 cells showed reductions in the center response to both contrasts, excitatory and inhibitory ($p < 0.05$, K-S test), four cells showed a change in only the inhibitory contrast response, and two cells showed no change in either response contrast. These data are represented again in Figure 6*I* grouped by whether the contrast was excitatory (+) or inhibitory and the population quantification is shown below in Figure 6*J*. Therefore, changes in both ON- and OFF-center response magnitude combine to yield changes in dLGN cell responsiveness with no change in RF size.

Not all cells had sufficient surround pixels above the noise to measure changes in RF surround magnitude. When non-noise surround pixels were observed (10/37), we also measured changes in the strength of the surround by considering pixels in ON- or OFF-center responses that were opposite sign to the center. We averaged the effect of removing Ntsr1 input and found that the strength of surround reduction correlated with the strength of center reduction, for both ON- and OFF-center responses (Fig. 6*K*). Surround reductions were not significantly different from those triggered from the center ($p = 0.96$, K-S test). We did not see evidence that dLGN surrounds were more affected by Ntsr1 projections than dLGN RF centers. Therefore, because the surround and the inhibitory center are mediated by interneurons, our results suggest that Ntsr1 input modulates relay and interneurons similarly.

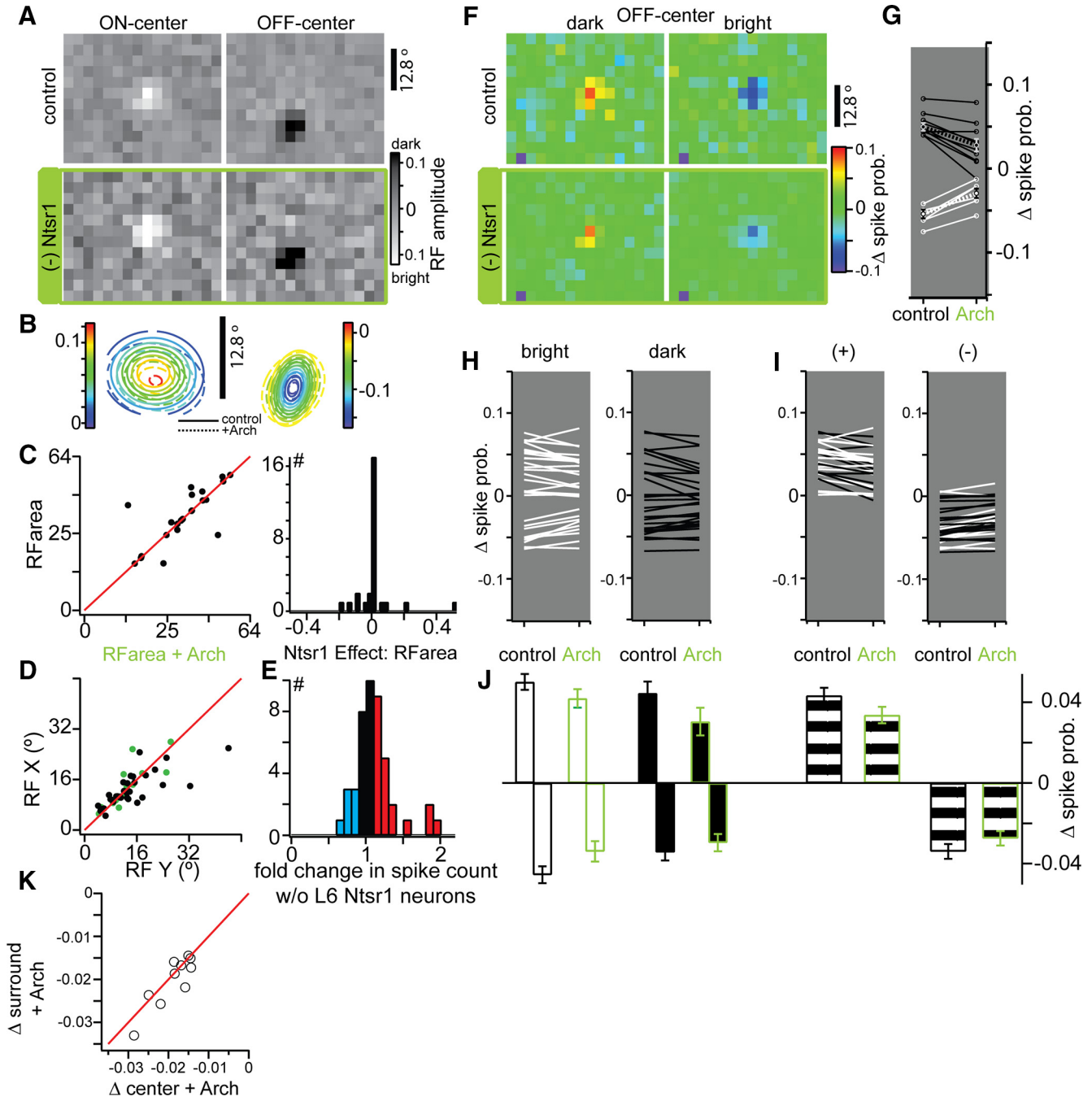

Figure 6. Effect of Ntsr1 cells on dLGN spatial RFs. ***A***, Spatial RFs for an ON-center (left) and OFF-center (right) unit in control (top) and +Arch (bottom) conditions. ***B***, 2D Gaussian fits of example cells in ***A*** for both control (solid contour lines) and +Arch (dashed contour lines). ***C***, Scatter plot showing the effect of Ntsr1 cells on RF area calculated from fit parameters (right) and the distribution of this effect (left). ***D***, Scatter plot of X and Y parameters of in control (black) and +Arch (green) conditions. ***E***, Distribution of the change in total number of spikes during ternary noise stimulation. ***F***, Bright-only (left) and dark-only (right) RFs in control (top) and +Arch (bottom) for an OFF-center cell. ***G***, Pixel-specific changes in non-noise pixels in the dark RF (black) and bright RF (white). Averages and SEM for each are connected by a dashed line. ***H***, Average changes in bright (left) and dark (right) pixels for all cells. ***I***, Average changes in pixels that increase spike probability (left) and decrease spike probability (right). ***J***, Average change in spike probability from plots in ***H***; cells are split by ON-center and OFF-center for solid plots and combined for striped plots. ***K***, Scatter plot of changes in surround versus changes in center strength measured with and without Arch activation. Center pixels are contiguous non-noise pixels and surround measured from all non-noise pixels adjacent to a non-noise center pixel.

RF time course

The impulse response measured at the pixel under the centroid of the Gaussian fit was not modified by removing Ntsr1 input (Fig. 7*A*, same two example cells as Fig. 6*A*). From each impulse response ($n = 35$), we measured the time of the peak (Fig. 7*B*), the amplitude of the peak (Fig. 7*C*), and the area under the rectified impulse response curve (Fig. 7*D*). The distributions in the right column (Fig. 7*B–D*) represent the difference between control and +Arch and they are centered at zero. Therefore, none of these parameters showed differences between control and +Arch (Fig. 7*B–D*).

We measured the temporal profile of the response at selected pixels within the RF estimated by reverse correlation. At the pixel with maximum response in the RF center (Fig. 7*E*, pixel 1, solid

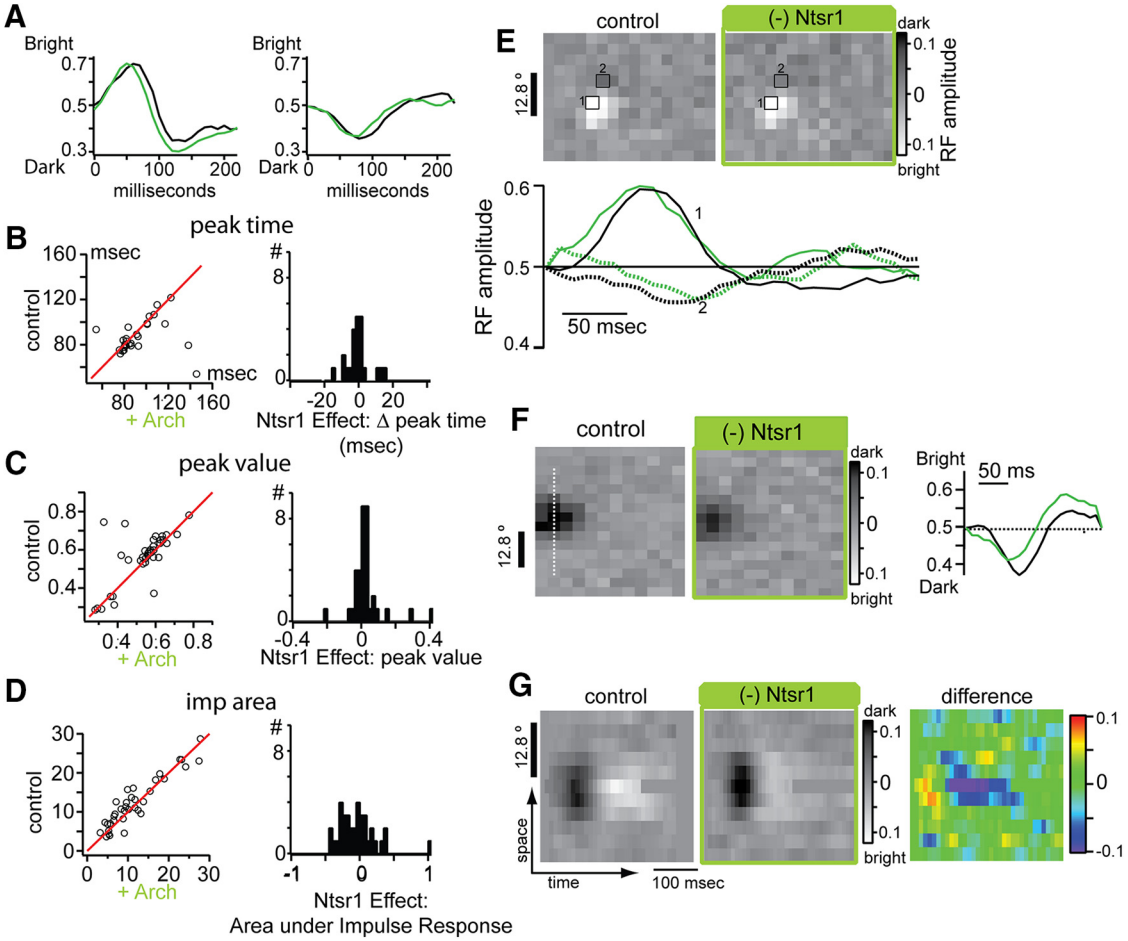

Figure 7. Effect of Ntsr1 cells on dLGN temporal RFs. ***A***, Example impulse responses for and ON-center (left) and OFF-center (right), with (black) and without (green) Ntsr1 cell activity. ***B–D***, Scatter plots (left) and corresponding distributions of effects of Ntsr1 cells for the time of impulse response peak (***B***), the value at that peak (***C***), and the absolute area under the impulse response (***D***). ***E***, Comparison of impulse responses from a center pixel and a surround pixel, with (black) and without (green) Ntsr1 cell activity. ***F***, ***G***, Space–time plot does not reveal any changes in temporal structure with (black) and without (green) Ntsr1 cell activity for the example cell shown in ***F***.

lines in impulse responses) and at points in the RF surround (Fig. 7*E*, pixel 2, dotted lines), we saw minimal change in the time course of the impulse response after removal of Ntsr1 input. To ensure that we were not missing any temporal effects by measuring impulse responses from individual pixels, we computed space–time RFs across several 1D slices of the RF. The example cell in Figure 7*F* showed a reduction in the magnitude of the response to dark stimuli in the RF center (in agreement with the results in Fig. 6), which was obvious in 2D RF plots and the impulse response with no change in time course of the response. The space–time RF for this cell (Fig. 7*G*, space axis indicated by dotted line in Fig. 7*F*) revealed that both the dark and bright responses were reduced in magnitude, as shown in the color-coded difference plot (Fig. 7*G*, right), but there was no change in the temporal dynamics of the response.

In summary, Ntsr1 input modulates response magnitude without changing the spatiotemporal properties of the RF of dLGN neurons. Furthermore, center and surround response magnitude were equally affected by Ntsr1 input, inconsistent with the notion that spatial arrangement controls the sign of the CT effect (Tsumoto et al., 1978).

Ntsr1 cells affect dLGN coordinated activity

The coincident activity of dLGN cells affects transmission of retinal input to V1 (Alonso et al., 1996; Usrey et al., 2000; Cardin et al., 2010a; Wang et al., 2010), can provide extra stimulus information (Dan et al., 1998; Reich et al., 2001), and may be influenced by cortical activity (Sillito et al., 1994; Sillito and Jones, 2002; Andolina et al., 2007). In addition, thalamic synchrony is a key component of sleep and anesthesia oscillations and is coordinated by CT input (Contreras et al., 1996). Low spontaneous firing rates precluded quantification of the role of Ntsr1 input to LGN synchrony during spontaneous activity and we focused our experiments on visually driven activity. To test whether Ntsr1 input regulates the coordinated visual responses of pairs of dLGN cells, we calculated cross-correlograms (CCGs; $n = 392$ pairs from 10 experiments) from the responses to drifting gratings of fixed orientation, spatial frequency, and temporal frequency while activating Arch in Ntsr1 cells on interleaved trials. In both control and +Arch conditions, CCGs showed a robust modulation at the frequency of the drifting grating (Fig. 8*A*, three example cells). The phase of this modulation, measured from the position of the CCG peak (Fig. 8*A*), depends on the relative spatial locations of the dLGN cell RFs (Andolina et al., 2007; Stanley et al., 2012); this phase was not altered by elimination of Ntsr1 projections (Fig. 8*B*), consistent with a lack of changes in spatial properties in +Arch condition (as shown in Fig. 5). We quantified the effect of removing Ntsr1 input on the CCG by measuring the area under the curve within ± 20 ms at two points: at time 0 (Fig. 8*C*, represented by the rectangle), which represents the nor-

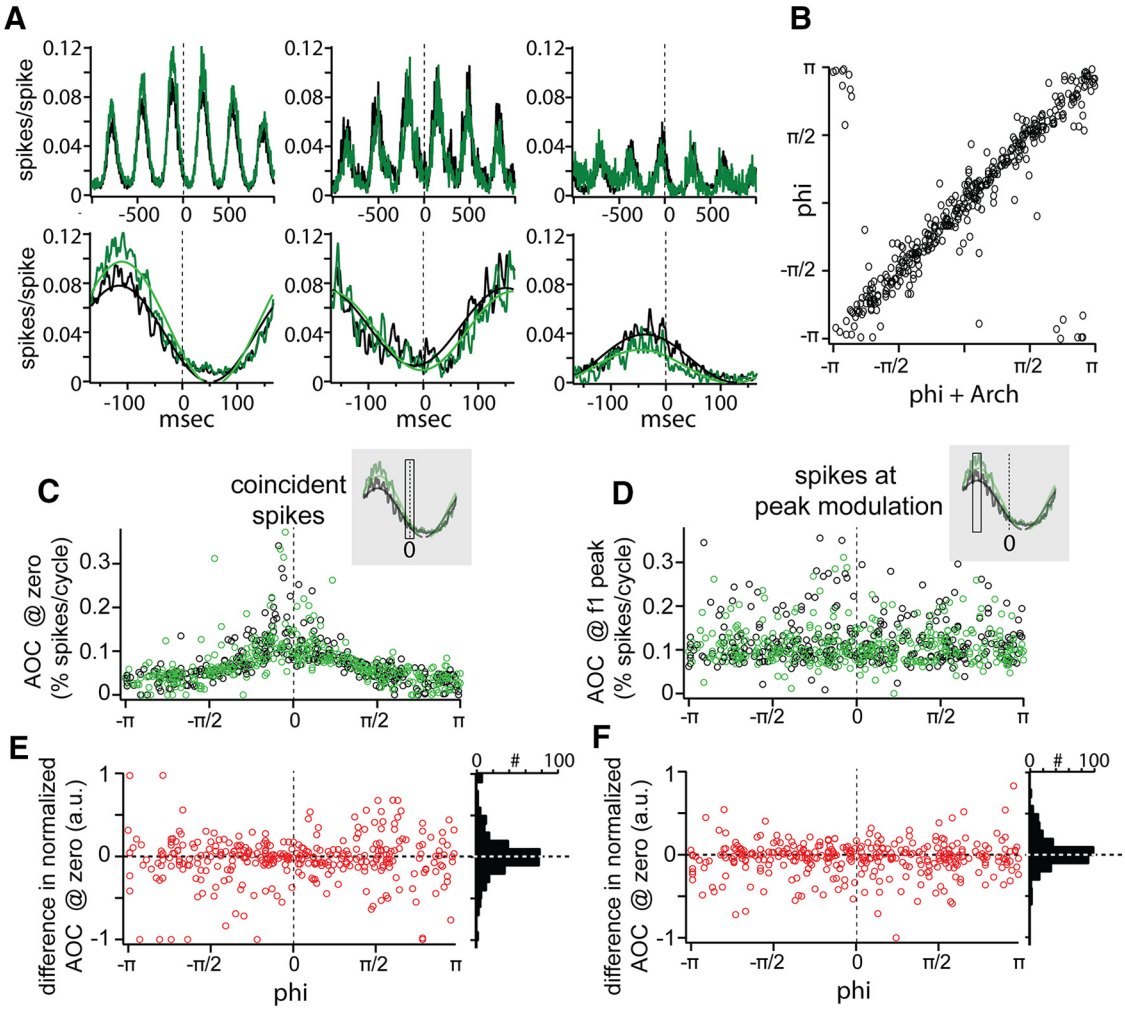

Figure 8. Effects of Ntsr1 cells of dLGN pairwise coordinated activity. ***A***, Three example pairs with modulating correlated activity that is increased (left), unchanged (middle), or reduced (right) by reduction in Ntsr1 firing. ***B***, Phase of the pairwise modulation is unchanged by Ntsr1 cell activity. ***C***, Area under the cross-correlation in the nonlinear summation window (±10 ms) as a function of the phase of cross-correlation modulation. ***D***, Area under the cross-correlation at the first peak of the cross-correlation as a function of the phase of modulation. ***E***, Difference in area under the curve between control and +Arch conditions in ***C***. ***F***, difference in area under the curve between control and +Arch conditions in ***D***.

malized amount of coincident spikes between the two neurons, and at the peak of the CCG, which represents the largest amount of correlated spikes between the two neurons (Fig. 8*D*). We plotted this magnitude as a function of the phase of the CCG for both control (in black) and +Arch (in green). As was expected from the effect on single dLGN units, the effect on CCGs was heterogeneous, with pairs exhibiting a range of increases and decreases in the percentage spikes at the center of the CCG (Fig. 8*C*). Furthermore, the change in the number of synchronous spikes was not dependent on the phase of the modulation, as shown by the distribution of the differences in peak amplitude between control and +Arch for all phases along the stimulus cycle (Fig. 8*E*, red dots); the distribution of changes in synchrony area was centered on zero (Fig. 8*E*, distribution at right). Likewise, changes in correlated spikes, that is, those at the peak of the CCG modulation regardless of the peak phase were also variable and independent of phase (Fig. 8*D*,*F*), as expected from a lack of change in modulation phase in individual units (Fig. 3). Together, the CCG results indicate that the Ntsr1 modulates coordinated activity, and thus the efficiency of retinal transfer, bidirectionally. This modulation is, at least within the range of our stimulus size, uniform in space (Fig. 8*F*).

To address the proposed role of CT input in selectively synchronizing dLGN cells linked by stimulus features (Sillito et al., 1994), we measured pairwise synchrony of dLGN units as function of the orientation of drifting gratings with and without Ntsr1 input ($n = 45$ CCGs from four experiments; Fig. 9). As described above, dLGN unit pair CCGs modulated at the temporal frequency of the grating (Fig. 9*A*) and, as shown by the example cells in Figure 9, *A* and *B*, in this case, the phase of the modulation shifted with the orientation of the grating. Synchronous activity was not dependent on the orientation of the grating (Fig. 9*B*), inconsistent with a role for CT input in selectivity synchronizing dLGN cells only for stimuli with a linking spatial feature. Suppression of Ntsr1 input did not change the area under the center of the CCG at any phase (Fig. 9*C*) and neither did it change the peak time regardless of CCG peak phase (Fig. 9*D*). In some CCGs (8/45), we also observed a gamma frequency entrainment between the cells; this gamma entrainment was also not stimulus specific (Fig. 9*F*), inconsistent with the interpretation of gamma entrainment as a feature-binding mechanism (Singer, 2001).

Ntsr1 cells do not control thalamic firing mode

Given the net inhibition caused by activation of the Ntsr1 population, we wondered whether removing Ntsr1 corticogeniculate projections could alter the prevalence of spike bursts. A change in firing mode, or in the proportion of T-channel activity, could

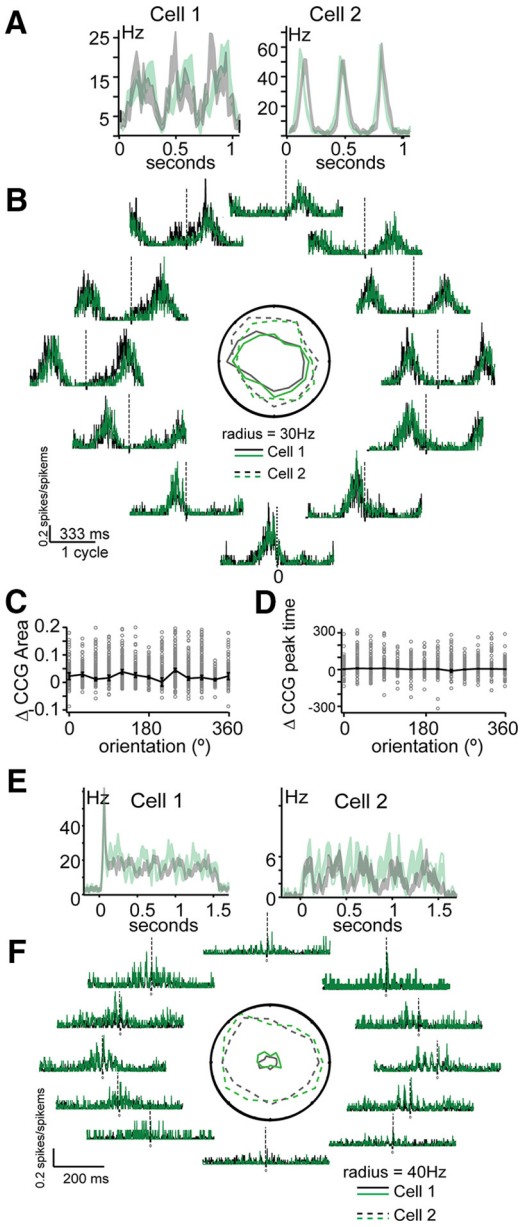

Figure 9. No stimulus dependence of Ntsr1 effects on coordinated activity. ***A***, Drifting grating responses of two simultaneously recorded units Peristimulus time histograms calculated with 33 ms bins for control (gray) and +Arch (green) are shown with SEM for each bin shaded. ***B***, Orientation tuning of the units shown in ***A*** (center polar plot); cross-correlation of the responses at each orientation showing procession of modulation peak, but no change in peak area or time with + Arch (in green) at any orientation. ***C***, ***D***, There is no consistent change between control and + Arch in peak area and peak time across all orientations for the population of simultaneously recorded pairs. ***E***, Drifting grating responses of two simultaneously recorded units. Control (gray) and +Arch (green) are shown with SEM shaded. ***F***, Orientation tuning of the units shown in ***E*** (center polar plot, legend as in ***B***); cross-correlation of the responses at each orientation showing no change in gamma frequency modulation as a function of orientation.

result in more visually evoked spikes even if Ntsr1 cells were providing a net inhibition. Moreover, cortical activity has been shown to affect dLGN interspike interval (ISI) distribution (Wörgötter et al., 2002). To measure dLGN firing mode, we constructed composite ISI plots to distinguish tonic and burst spikes. Composite ISIs were generated by plotting, for each spike, the subsequent ISI versus the previous ISI. Bursts, due to a low threshold spike, generate a characteristic set of three clusters: the first spike in each burst is preceded by a long ISI (>100 ms) and followed by a short ISI (<4 ms) (Fig. 10*A*, Zone 1); the spike at the end of each burst is preceded by a short (<4 ms) and followed by a long (>100 ms) ISI (Fig. 10*A*, Zone 3). Within bursts were characterized by both preceding and following short ISIs (<4 ms; Fig. 10*A*, Zone 2). All other spikes are treated as tonic firing.

The three example cells in Figure 10*A* illustrate critical points about spike firing patterns in mouse dLGN. First, the three cells recorded simultaneously responded to drifting gratings with a large proportion of spike bursts (Fig. 10*A*, left ISI), predominant tonic firing (Fig. 10*A*, right ISI), or a combination of both (Fig. 10*A*, middle ISI). Second, the three cells largely preserve their distinction in firing pattern in response to a very different visual stimulus such as a flicker stimulus (Fig. 10*D*).

By interleaving control and Arch trials, we were able to compare quantitatively the proportion of bursting with and without Ntsr1 input. In the examples cells in Figure 10, the distribution of ISIs in the visual responses to gratings and the flicker stimuli were not modified in the absence of Ntsr1 input (Fig. 10*A*,*B*, green dots). We summed the intervals falling within Zones 1, 2, and 3 to calculate the percent bursting within the entire visual response in each cell. The comparison of percent bursting in control and +Arch during the response to gratings (Fig. 10*B*,*C*) and the response to the flicker stimulus (Fig. 10*E*,*F*) was similar because the vast majority of neurons lie along the main diagonal of the scatter plots.

In conclusion, the observed changes in visual responsiveness in the absence of Ntsr1 input indicate that Ntsr1 corticogeniculate projections drive a mix of inhibition and excitation depending on the dLGN cell target and level of Ntsr1 cell activation. Whereas activation of Ntsr1 input with ChR2 generates almost exclusively inhibitory responses in dLGN (Fig. 1), removal of Ntsr1 cell input does not lead to clear disinhibition because we did not observe a shift from bursting to tonic nor a change in the percentage of bursts in visual responses.

Discussion

We found Ntsr1-Cre corticogeniculate projections to be capable of driving both increases and decreases in dLGN spike counts during visually evoked activity, likely via a mixture of indirect inhibition and direct excitation. Tuning properties suggest wide convergence of Ntsr1 cells with similar contrast, spatial, and temporal frequency tuning onto single dLGN cells. We did not find evidence that Ntsr1 cells sharpen spatial tuning properties or improve temporal fidelity. Finally, we found that Ntsr1 cells can affect retinal transfer in a way consistent and predicted by the effects on single cells.

Anatomical correlates of Ntsr1 cell classification

Previous investigation of CT projections have relied on gross manipulations of cortical activity. Here, we restricted our manipulation to a more specific cell type, the Ntsr1 population. Ntsr1 cells are a genetically defined class, as opposed to the many anatomically (Tombol, 1984) or physiologically defined (Briggs and Usrey, 2009) L6 cell classes (Thomson, 2010). Based on the morphology of Nstr1 cells (Figs. 1, 2; Olsen et al., 2012) and distribution of subcortical targets, Ntsr1 cells represent at least two L6 cell classes: upper L6 dLGN-specific and lower L6 dLGN- and LP-projecting cells (Bourassa and Deschênes, 1995; Zhang and Deschênes, 1997). These morphological classes correlate with the "type I" and "type II" classifications based on morphology and the pattern of local cortical input (Zarrinpar and Callaway, 2006). Ntsr1 cells are orientation selective and responses modulate strongly at the drifting grating frequency (Fig. 2*D*), consistent with a simple RF structure.

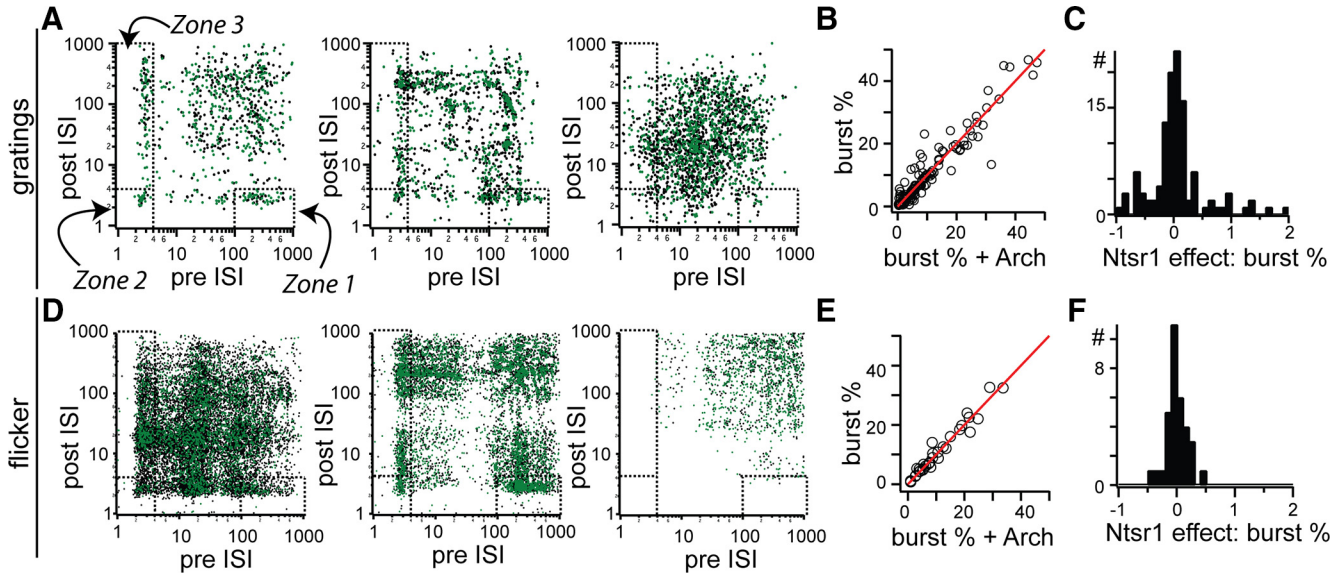

Figure 10. No change in dLGN burst statistics due to Ntsr1 cell activity. ***A***, Composite interspike interval plots for three example cells generated from spike responses to drifting gratings. Burst spikes fall in the zones demarcated by dashed lines and indicated with curved arrows. ***B***, ***C***, Scatter plot of percentage of burst spikes in control and +Arch conditions (***B***) and the corresponding distribution (***C***). ***D***, Composite ISI plots for three example cells generated from spike responses to spatially uniform flicker. ***E***, ***F***, Scatter plot of percentage of burst spikes in control and +Arch conditions (***E***) and the corresponding distribution (***F***).

Diversity of spike count effects

Whereas some previous studies have reported a diversity of spike count effects from manipulations of CT projections (Molotchnikoff and Lachapelle, 1977; McClurkin et al., 1994), others have focused on increases or decreases. What could account for the diversity in spike count effects? Intracellular recordings show that activation of Ntsr1 results in both excitation and inhibition in thalamic relay neurons (Mease et al., 2014). One hypothesis to account for the diversity in spike count effects in the visual (Tsumoto et al., 1978; Marrocco and McClurkin, 1985) and other CT systems (Li and Ebner, 2007, Temereanca and Simons, 2004) is the alignment of the feedback. According to this hypothesis, the effects of CT cells with spatially aligned RF centers are excitatory, whereas CT cells centered in the dLGN cell surround provide a net inhibition. Here, we manipulated all Ntsr1 corticogeniculate projections regardless of the spatial arrangement with the recorded cells in dLGN. Nevertheless, we did not observe any nonuniformities in Ntsr1 effects during noise stimulation, which would be expected if CT projections in different spatial regions provided opposing effects. More direct testing of this hypothesis may require spatial control of the optogenetic manipulation such that only center-aligned or only surround corticogeniculate cells are manipulated; such arbitrary spatiotemporal specificity is achievable by combining optogenetics with modified digital light projection optical systems (Stirman et al., 2012).

Given the parallel population of relay cells in primate and cat dLGN, it is possible that the diversity of Ntsr1 effect could be correlated with dLGN cell type. To date, only morphological evidence indicates a homology to X/Y types (Krahe et al., 2011), with functional studies of single cells finding very little evidence for magno/parvo or X/Y type homology (Grubb and Thompson, 2003; Piscopo et al., 2013). Because of the lack of physiological identifier, we were unable to test whether any of the observed variance can be attributed to separate, parallel channels in dLGN. Other evidence from rodents suggests multiple populations (Sumitomo et al., 1969; Hale et al., 1979; Lennie and Perry, 1981), so it remains possible that parallel mouse dLGN streams could be affected differently by Ntsr1 projections, perhaps with release of inhibition to high-velocity stimuli (Gulyás et al., 1990; Hawken et al., 1996; Fig. 4).

Anesthetic state can have strong effects on thalamic and cortical function (Angel and LeBeau, 1992; Briggs and Usrey, 2008). However, we do not believe that fluctuations in anesthetic state can account for the diversity in Ntsr1 effects on thalamic responses for two primary reasons: cells recorded simultaneously, and therefore in the same "anesthetic state," displayed diverse effects (Fig. 3*A*,*B*) and analysis of the spectral content of local field potentials from the recording showed little range, indicating a similar state across experiments. Slow oscillations were absent and epochs with 4–8 Hz spindles (Contreras and Steriade, 1996) were rare, consistent with a mostly nonsynchronized thalamocorticothalamic system with little or no thalamic bursting (Fig. 10*B*,*E*).

Gain

Ntsr1 cells are visually responsive (Fig. 2) and their spike count increases with increasing stimulus contrast. In dLGN, we observed changes in Ntsr1-mediated spike count effect that scaled with the contrast of the visual stimulus (Fig. 3). This scaling of Ntsr1-mediated effect with contrast could be interpreted as a gain control (Olsen et al., 2012) or it could be interpreted as a scaling of the Ntsr1 effect with the gain of system. In this sense, Ntsr1 cells may not be implementing gain control in the thalamus (Saalmann and Kastner, 2009), but rather providing a change in spike count that itself is also gain controlled.

Regulation of retinal transfer, RF spatial extent, and temporal properties

Our cross-correlation data indicate that Ntsr1 cells can both increase and decrease visually driven thalamic synchrony. Synchronous spikes, occurring within 10 ms of each other, are more effective at driving downstream cortical activity (Cardin et al., 2010a; Wang et al., 2010) and are upregulated and downregulated by Ntsr1 activity (Fig. 8). The present data do not address under what condition, or toward what end, such regulation would occur.

We did not find evidence that Ntsr1 cells sharpen spatial tuning properties or improve temporal fidelity, suggesting that cortical influences on these dLGN response features either use another channel or are species specific. It is possible that surround effects require more effective engagement of the surround than our stimuli provided. Our stimuli are limited by the size of the monitor, which may not always be large enough for mouse RFs, especially given that the stimuli are tailored for only a subset of the many cells recorded using our mutlitetrode approach. Early experiments indicated that removal of Ntsr1 input did not change the magnitude of surround effects on cortical responses, so we did not explore this interaction of grating size and Ntsr1 activity further in dLGN. Finally, changes in neuromodulation caused by cortical manipulation of non-CT cells could account for increase in stimulus information reported in other studies (Wörgötter et al., 1998; Andolina et al., 2007; Goard and Dan, 2009).

Putative mechanisms

Consistent with the reduction in dLGN spiking generated by electrical (Marrocco et al., 1982; Ahlsén et al., 1985) or transcranial magnetic stimulation of V1 (de Labra et al., 2007), as well as previous reports in the mouse visual system (Olsen et al., 2012), we found that synchronous activation of Ntsr1 cells elicits reduction in spike count, presumably through activation of RE or local inhibitory input to dLGN relay cells. However, Ntsr1 activity does not always result in net inhibition, as evidenced by our Arch experiments removing Ntsr1 activity. We propose that Ntsr1 effects are a balance of monosynaptic excitation and disynaptic inhibition that can be tipped toward either inhibition or excitation. Synchronous activation results in a large inhibition. These results highlight the usefulness of pairing gain-of-function and loss-of-function optogenetic experiments.

An alternative possible explanation for a decrease in thalamic spike count is the change in firing mode from burst to tonic, whereby a depolarization would reduce the number to burst spike evoked by an excitatory input (Guido and Weyand, 1995). According to this hypothesis, manipulating Ntsr1 projections should create changes in burst frequency or magnitude. Unlike other reports (Mease et al., 2014), we did not see evidence of a change in either burst frequency or magnitude in the absence of Ntsr1 cell activity (Fig. 10). The diverse effects of Ntsr1 cells may also be mediated by a more complex polysynaptic mechanism, given than Ntsr1 cells make synaptic connections to translaminar cortical inhibitory cells (Bortone et al., 2014) and excitatory cells in L4 and L5a (Kim et al., 2014).

Nonsensory functions of CT projections

CT projections have been hypothesized to participate in several nonsensory functions such as spindles (Contreras and Steriade, 1996), seizures (McCormick and Contreras, 2001), and the sleep–wake transition (Steriade and Timofeev, 2003). We did not observe sufficient spontaneous, non-visually-driven spiking to quantify the effects of Ntsr1 neurons directly in concerted oscillatory thalamic activity. However, our data support the role of corticotgeniculate projections in absence seizures because strong synchronous activity of Ntsr1 cells could inhibit thalamic activity deeply, although the visual stimuli that we used are not sufficient to tip the balance toward strong and pathologic thalamic inhibition. The bidirectional effects limit what role these cells might have in generating an oscillation; Ntsr1 cells did not specifically affect the pairwise gamma oscillations (Fig. 9). We propose that, like its sensory effects, the effects of Ntsr1 on oscillations are general and mixed.

References

Ahlsén G, Lindström S, Lo FS (1985) Interaction between inhibitory pathways to principal cells in the lateral geniculate nucleus of the cat. Exp Brain Res 58:134–143. Medline

Alonso JM, Usrey WM, Reid RC (1996) Precisely correlated firing in cells of the lateral geniculate nucleus. Nature 383:815–819. CrossRef Medline

Andolina IM, Jones HE, Wang W, Sillito AM (2007) Corticothalamic feedback enhances stimulus response precision in the visual system. Proc Natl Acad Sci U S A 104:1685–1690. CrossRef Medline

Andolina IM, Jones HE, Sillito AM (2013) Effects of cortical feedback on the spatial properties of relay cells in the lateral geniculate nucleus. J Neurophysiol 109:889–899. CrossRef Medline

Angel A, LeBeau F (1992) A comparison of the effects of propofol with other anaesthetic agents on the centripetal transmission of sensory information. Gen Pharmacol 23:945–963. CrossRef Medline

Atasoy D, Aponte Y, Su HH, Sternson SM (2008) A FLEX switch targets channelrhodopsin-2 to multiple cell types for imaging and long-range circuit mapping. J Neurosci 28:7025–7030. CrossRef Medline

Baker FH, Malpeli JG (1977) Effects of cryogenic blockade of visual cortex on the responses of lateral geniculate neurons in the monkey. Exp Brain Res 9:433–444.

Bortone DS, Olsen SR, Scanziani M (2014) Translaminar inhibitory cells recruited by layer 6 corticothalamic neurons suppress visual cortex. Neuron 82:474–485. CrossRef Medline

Bourassa J, Deschênes M (1995) Corticothalamic projections from the primary visual cortex in rats: a single fiber study using biocytin as an anterograde tracer. Neuroscience 66:253–263. CrossRef Medline

Briggs F (2010) Organizing principles of cortical layer 6. Front Neural Circuits 4:3. Medline

Briggs F, Usrey WM (2008) Emerging views of corticothalamic function. Curr Opin Neurobiol 18:403–407. CrossRef Medline

Briggs F, Usrey WM (2009) Parallel processing in the corticogeniculate pathway of the macaque monkey. Neuron 62:135–146. CrossRef Medline

Carandini M, Heeger DJ (2012) Normalization as a canonical neural computation. Nat Rev Neurosci 13:51–62. Medline

Carandini M, Heeger DJ, Movshon JA (1997) Linearity and normalization in simple cells of the macaque primary visual cortex. J Neurosci 17:8621–8644. Medline

Cardin JA, Kumbhani RD, Contreras D, Palmer LA (2010a) Cellular mechanisms of temporal sensitivity in visual cortex neurons. J Neurosci 30:3652–3662. CrossRef Medline

Cardin JA, Carlén M, Meletis K, Knoblich U, Zhang F, Deisseroth K, Tsai LH, Moore CI (2010b) Targeted optogenetic stimulation and recording of neurons in vivo using cell-type-specificexpression of channelrhodopsin-2. Nat Protoc 5:247–254. CrossRef Medline

Chow BY, Han X, Dobry AS, Qian X, Chuong AS, Li M, Henninger MA, Belfort GM, Lin Y, Monahan PE, Boyden ES (2010) High-performance genetically targetable optical neural silencing by light-driven proton pumps. Nature 463:98–102. CrossRef Medline

Contreras D, Palmer L (2003) Response to contrast of electrophysiologically defined cell classes in primary visual cortex. J Neurosci 23:6936–6945. Medline

Contreras D, Steriade M (1996) Spindle oscillation in cats: the role of corticothalamic feedback in a thalamically generated rhythm. J Physiol 490:159–179. CrossRef Medline

Crunelli V, Haby M, Jassik-Gerschenfeld D, Leresche N, Pirchio M (1988) Cl- - and K+-dependent inhibitory postsynaptic potentials evoked by interneurones of the rat lateral geniculate nucleus. J Physiol 399:153–176. Medline

Dan Y, Alonso JM, Usrey WM, Reid RC (1998) Coding of visual information by precisely correlated spikes in the lateral geniculate nucleus. Nat Neurosci 1:501–507. CrossRef Medline

de Labra C, Rivadulla C, Grieve K, Mariño J, Espinosa N, Cudeiro J (2007) Changes in visual responses in the feline dLGN: selective thalamic suppression induced by transcranial magnetic stimulation of V1. Cereb Cortex 17:1376–1385. CrossRef Medline

Denman DJ, Contreras D (2014) The structure of pairwise correlation in mouse primary visual cortex reveals functional organization in the absence of an orientation map. Cereb Cortex 24:2707–2720. CrossRef Medline

Destexhe A, Contreras D, Steriade M (1998) Mechanisms underlying the synchronizing action of corticothalamic feedback through inhibition of thalamic relay cells. J Neurophysiol 79:999–1016. Medline

Gao E, DeAngelis GC, Burkhalter A (2010) Parallel input channels to mouse primary visual cortex. J Neurosci 30:5912–5926. CrossRef Medline
Goard M, Dan Y (2009) Basal forebrain activation enhances cortical coding of natural scenes. Nat Neurosci 12:1444–1449. CrossRef Medline
Gong S, Doughty M, Harbaugh CR, Cummins A, Hatten ME, Heintz N, Gerfen CR (2007) Targeting Cre recombinase to specific neuron populations with bacterial artificial chromosome constructs. J Neurosci 27:9817–9823. CrossRef Medline
Grubb MS, Thompson ID (2003) Quantitative characterization of visual response properties in the mouse dorsal lateral geniculate nucleus. J Neurophysiol 90:3594–3607. CrossRef Medline
Guido W, Weyand T (1995) Burst responses in thalamic relay cells of the awake behaving cat. J Neurophysiol 74:1782–1786. Medline
Gulyás B, Lagae L, Eysel U, Orban GA (1990) Corticofugal feedback influences the responses of geniculate neurons to moving stimuli. Exp Brain Res 79:441–446. CrossRef Medline
Hale PT, Sefton AJ, Dreher B (1979) A correlation of receptive field properties with conduction velocity of cells in the rat's retino-geniculo-cortical pathway. Exp Brain Res 35:425–442. Medline
Hawken MJ, Shapley RM, Grosof DH (1996) Temporal-frequency selectivity in monkey visual cortex. Vis Neurosci 13:477–492. CrossRef Medline
Hull EM (1968) Corticofugal influence in the macaque lateral geniculate nucleus. Vis Res 8:1285–1298. CrossRef Medline
Jones E (2007) The thalamus, Vol 2. Cambridge: Cambridge University.
Jurgens CW, Bell KA, McQuiston AR, Guido W (2012) Optogenetic stimulation of the corticothalamic pathway affects relay cells and GABAergic neurons differently in the mouse visual thalamus. PLoS One 7:e45717. CrossRef Medline
Kalil RE, Chase R (1970) Corticofugal influence on activity of lateral geniculate neurons in the cat. J Neurophysiol 33:459–474. Medline
Kim J, Matney CJ, Blankenship A, Hestrin S, Brown SP (2014) Layer 6 corticothalamic neurons activate a cortical output layer, layer 5a. J Neurosci 34:9656–9664. CrossRef Medline
Krahe TE, El-Danaf RN, Dilger EK, Henderson SC, Guido W (2011) Morphologically distinct classes of relay cells exhibit regional preferences in the dorsal lateral geniculate nucleus of the mouse. J Neurosci 31:17437–17448. CrossRef Medline
Kumbhani RD, Nolt MJ, Palmer LA (2007) Precision, reliability, and information-theoretic analysis of visual thalamocortical neurons. J Neurophysiol 98:2647–2663. CrossRef Medline
Lennie P, Perry VH (1981) Spatial contrast sensitivity of cells in the lateral geniculate nucleus of the rat. J Physiol 315:69–79. CrossRef Medline
Li L, Ebner FF (2007) Cortical modulation of spatial and angular tuning maps in the rat thalamus. J Neurosci 27:167–179. CrossRef Medline
Marrocco RT, McClurkin JW (1985) Evidence for spatial structure in the cortical input to the monkey lateral geniculate nucleus. Exp Brain Res 59:50–56. Medline
Marrocco RT, McClurkin JW, Young RA (1982) Modulation of lateral geniculate cell responsiveness by visual activation of the corticogeniculate pathway. J Neurosci 2:256–263. Medline
McClurkin JW, Optican LM, Richmond BJ (1994) Cortical feedback increases visual information transmitted by monkey parvocellular lateral geniculate nucleus neurons. Vis Neurosci 11:601–617. CrossRef Medline
McCormick DA, Contreras D (2001) On the cellular and network bases of epileptic seizures. Annu Rev Physiol 63:815–846. CrossRef Medline
McCormick DA, von Krosigk M (1992) Corticothalamic activation modulates thalamic firing through glutamate "metabotropic" receptors. Proc Natl Acad Sci U S A 89:2774–2778. CrossRef Medline
McCormick DA, Pape HC (1990) Properties of a hyperpolarization-activated cation current and its role in rhythmic oscillation in thalamic relay neurones. J Physiol 431:291–318. CrossRef Medline
Mease RA, Krieger P, Groh A (2014) Cortical control of adaptation and sensory relay mode in the thalamus. Proc Natl Acad Sci U S A 111:6798–6803. CrossRef Medline
Molotchnikoff S, Lachapelle P (1977) Corticofugal influence on evoked activity of lateral geniculate neurons in the rabbit. Exp Brain Res 29:527–530. Medline
Olsen SR, Bortone DS, Adesnik H, Scanziani M (2012) Gain control by layer six in cortical circuits of vision. Nature 483:47–52. CrossRef Medline
Piscopo DM, El-Danaf RN, Huberman AD, Niell CM (2013) Diverse visual features encoded in mouse lateral geniculate nucleus. J Neurosci 33:4642–4656. CrossRef Medline
Priebe NJ, Ferster D (2012) Mechanisms of neuronal computation in mammalian visual cortex. Neuron 75:194–208. CrossRef Medline
Przybyszewski AW, Gaska JP, Foote W, Pollen DA (1981) Striate cortex increases contrast gain of macaque LGN neurons. Vis Neurosci 17:485–494. Medline
Reich DS, Mechler F, Victor JD (2001) Independent and redundant information in nearby cortical neurons. Science 294:2566–2568. CrossRef Medline
Reinagel P, Reid RC (2000) Temporal coding of visual information in the thalamus. J Neurosci 20:5392–5400. Medline
Richard D, Gioanni Y, Kitsikis A, Buser P (1975) A study of geniculate unit activity during cryogenic blockade of the primary visual cortex in the cat. Exp Brain Res 22:235–242. Medline
Saalmann YB, Kastner S (2009) Gain control in the visual thalamus during perception and cognition. Curr Opin Neurobiol 19:408–414. CrossRef Medline
Sillito AM, Jones HE (2002) Corticothalamic interactions in the transfer of visual information. Philos Trans R Soc Lond B Biol Sci 357:1739–1752. CrossRef Medline
Sillito AM, Jones HE, Gerstein GL, West DC (1994) Feature-linked synchronization of thalamic relay cell firing induced by feedback from the visual cortex. Nature 369:479–482. CrossRef Medline
Singer W (2001) Consciousness and the binding problem. Ann N Y Acad Sci 929:123–146. Medline
Stanley GB, Jin J, Wang Y, Desbordes G, Wang Q, Black MJ, Alonso JM (2012) Visual orientation and directional selectivity through thalamic synchrony. J Neurosci 32:9073–9088. CrossRef Medline
Steriade M (2001) Impact of network activities on neuronal properties in corticothalamic systems. J Neurophysiol 86:1–39. Medline
Steriade M, Deschênes M (1984) The thalamus as a neuronal oscillator. Brain Res 320:1–63. Medline
Steriade M, Timofeev I (2003) Neuronal plasticity in thalamocortical networks during sleep and waking oscillations. Neuron 37:563–576. CrossRef Medline
Stirman JN, Crane MM, Husson SJ, Gottschalk A, Lu H (2012) A multispectral optical illumination system with precise spatiotemporal control for the manipulation of optogenetic reagents. Nat Protoc 7:207–220. CrossRef Medline
Sumitomo I, Ide K, Iwama K, Arikuni T (1969) Conduction velocity of optic nerve fibers innervating lateral geniculate body and superior colliculus in the rat. Exp Neurol 25:378–392. CrossRef Medline
Swindale NV (1998) Orientation tuning curves: empirical description and estimation of parameters. Biol Cybern 78:45–56. CrossRef Medline
Temereanca S, Simons DJ (2004) Functional topography of corticothalamic feedback enhances thalamic spatial response tuning in the somatosensory whisker/barrel system. Neuron 41:639–651. CrossRef Medline
Thomson AM (2010) Neocortical layer 6, a review. Front Neuroanat 4:13. CrossRef Medline
Tombol T (1984) Layer VI cells. In: Cereb cortex, Vol 1 (Peters A, Jones EG, eds), pp 479–519. New York: Plenum.
Tsumoto T, Creutzfeldt OD, Legéndy CR (1978) Functional organization of the corticofugal system from visual cortex to lateral geniculate nucleus in the cat. Exp Brain Res 32:345–364. Medline
Usrey WM, Alonso JM, Reid RC (2000) Synaptic interactions between thalamic inputs to simple cells in cat visual cortex. J Neurosci 20:5461–5467. Medline
Wang HP, Spencer D, Fellous JM, Sejnowski TJ (2010) Synchrony of thalamocortical inputs maximizes cortical reliability. Science 328:106–109. CrossRef Medline
Wörgötter F, Nelle E, Li B, Funke K (1998) The influence of corticofugal feedback on the temporal structure of visual responses of cat thalamic relay cells. J Physiol 509:797–815. CrossRef Medline
Wörgötter F, Eyding D, Macklis JD, Funke K (2002) The influence of the corticothalamic projection on responses in thalamus and cortex. Philos Trans R Soc Lond B Biol Sci 357:1823–1834. CrossRef Medline
Zarrinpar A, Callaway EM (2006) Local connections to specific types of layer 6 neurons in the rat visual cortex. J Neurophysiol 95:1751–1761. CrossRef Medline
Zhang ZW, Deschênes M (1997) Intracortical axonal projections of lamina VI cells of the primary somatosensory cortex in the rat: a single-cell labeling study. J Neurosci 17:6365–6379. Medline